Nonequilibrium Fluctuational Quantum Electrodynamics: Heat Radiation, Heat Transfer, and Force

Giuseppe Bimonte,[1,2] Thorsten Emig,[3,4] Mehran Kardar,[5] and Matthias Krüger[6,7]

[1]Dipartimento di Fisica E. Pancini, Università di Napoli Federico II, Complesso Universitario Monte Sant'Angelo, I-80126 Napoli, Italy

[2]Istituto Nazionale di Fisica Nucleare (INFN), Sezione di Napoli, I-80126 Napoli, Italy; email: bimonte@na.infn.it

[3]Multi-Scale Materials Science for Energy and Environment, The Joint CNRS-MIT Laboratory, Massachusetts Institute of Technology, Cambridge, Massachusetts 02139; email: emig@mit.edu

[4]Laboratoire de Physique Théorique et Modèles Statistiques, CNRS, Université Paris-Saclay, 91405 Orsay, France

[5]Department of Physics, Massachusetts Institute of Technology, Cambridge, Massachusetts 02139; email: kardar@mit.edu

[6]Fourth Institute for Theoretical Physics, Universität Stuttgart, 70569 Stuttgart, Germany

[7]Max Planck Institute for Intelligent Systems, 70569 Stuttgart, Germany; email: mkrueger@is.mpg.de

Annu. Rev. Condens. Matter Phys. 2017. 8:119–43

First published online as a Review in Advance on January 11, 2017

The *Annual Review of Condensed Matter Physics* is online at conmatphys.annualreviews.org

https://doi.org/10.1146/annurev-conmatphys-031016-025203

Keywords

fluctuational QED, Casimir force, near-field, scattering

Abstract

Quantum-thermal fluctuations of electromagnetic waves are the cornerstone of quantum statistics and inherent to phenomena such as thermal radiation and van der Waals forces. Although the principles are found in elementary texts, recent experimental and technological advances make it necessary to come to terms with counterintuitive consequences at short scales—the so-called near-field regime. We focus on three manifestations: (*a*) The Stefan–Boltzmann law describes radiation from macroscopic bodies but fails for small objects. (*b*) The heat transfer between two bodies at close proximity is dominated by evanescent waves and can be orders of magnitude larger than the classical (propagating) contribution. (*c*) Casimir forces, dominant at submicron separation, are not sufficiently explored for objects at different temperatures (at least experimentally). We explore these phenomena using fluctuational quantum electrodynamics (QED), introduced by Rytov in the 1950s, combined with scattering formalisms. This enables investigation of different material properties, shapes, separations, and arrangements.

1. INTRODUCTION

Blackbody: A body with emissivity of unity, marking the maximal value for planar surfaces

Skin depth, δ: Length scale of damping of waves inside matter

The beginnings of quantum mechanics can be traced back to the introduction of Planck's constant ($\hbar = h/2\pi$) for describing the spectrum of blackbody radiation at a given temperature T (1). Planck's law then leads to the well-known Stefan–Boltzmann law (2) for radiated power ($\propto \sigma T^4$, where σ is the Stefan–Boltzmann constant), and in turn to radiative heat transfer between objects at different temperatures [$\propto \sigma(T_1^4 - T_2^4)$]. To first approximation, everyday matter is held together by the fluctuating electromagnetic (EM) fields between (on average) neutral objects. At the atomic scale, this attractive interaction appears in the guises of van der Waals, Keesom, Debye, and London forces (3). At larger scales, the collective behavior of condensed atoms is better formulated in terms of dielectric properties. In 1948, Casimir computed the force between two perfectly conducting parallel plates that also arises due to the quantum fluctuations of the EM waves in the intervening vacuum (or, equivalently, due to the charge and current fluctuations in the plates) (4). This calculation was extended by Lifshitz to dielectric plates, accounting for the fluctuating currents in the media (5). Typically, at small separations quantum (zero-point) fluctuations shape the force, whereas at separations large compared to the thermal wavelength $\lambda_T = \hbar c/(2\pi k_B T)$ (approximately 1.2 μm at room temperature $T = 300$ K), thermal effects dominate and give rise to equilibrium or nonequilibrium Casimir forces (5–7).

Over the past two decades, there has been considerable progress in precision measurements of heat transfer and Casimir forces at submicron scale (8).[1] This growing interest can be attributed to the fact that heat transfer measurements are directly connected to scanning tunneling microscopy and scanning thermal microscopy, under ultra-high vacuum conditions (9, 10), whereas Casimir forces must be accounted for in the fabrication of micro- and nanoelectromechanical devices actuated by electrical bias (where this force is dominant). Thus, developing theoretical tools that allow treatment of systems out of thermal equilibrium is of particular relevance. Unlike the equilibrium case, concepts such as entropy and Helmholtz free energy (containing information about forces and torques) cannot be applied to systems out of thermal equilibrium. One approach is to apply the formalism of fluctuational electrodynamics (FE) introduced by Rytov (11) in the 1950s (12, 13). As discussed in Section 2, Rytov's formalism is based on the assumption of local equilibrium for each object and characterized by a temperature and dielectric response. The study of multiple objects of different shapes and material properties can be achieved by use of scattering methods (14–17), as explored in Section 3. Merging Rytov and scattering formalisms enables compactly representing radiation and forces in terms of scattering operators of the individual objects (14–17) as demonstrated in Section 4. Several applications of the results demonstrating the importance of size, shape, and geometry are provided in Section 5. Overall, the goal of this review is to illustrate the following novel twists on textbook results for heat and force, as summarized in **Figure 1**:

1. **Heat radiation** by objects with sizes smaller or comparable with the thermal wavelength is not accurately described by the Stefan–Boltzmann law. This occurs owing to interference effects between the object and the emitted radiation, such that its emissivity and absorptivity depend sensitively on its size and shape. Additionally, if the object is smaller than the penetration (skin) depth, the emitted power is proportional to the object's volume rather than its surface area. For example, **Figure 1*a*** depicts radiation from a silica nanofiber of diameter 500 nm; it displays good agreement together with the prediction of Equation 38 (below), unlike a naive computation using the Stefan–Boltzmann law (also shown in the figure).

[1] Parts of this review are taken with permission from the doctoral thesis of Dr. V.A. Golyk (8).

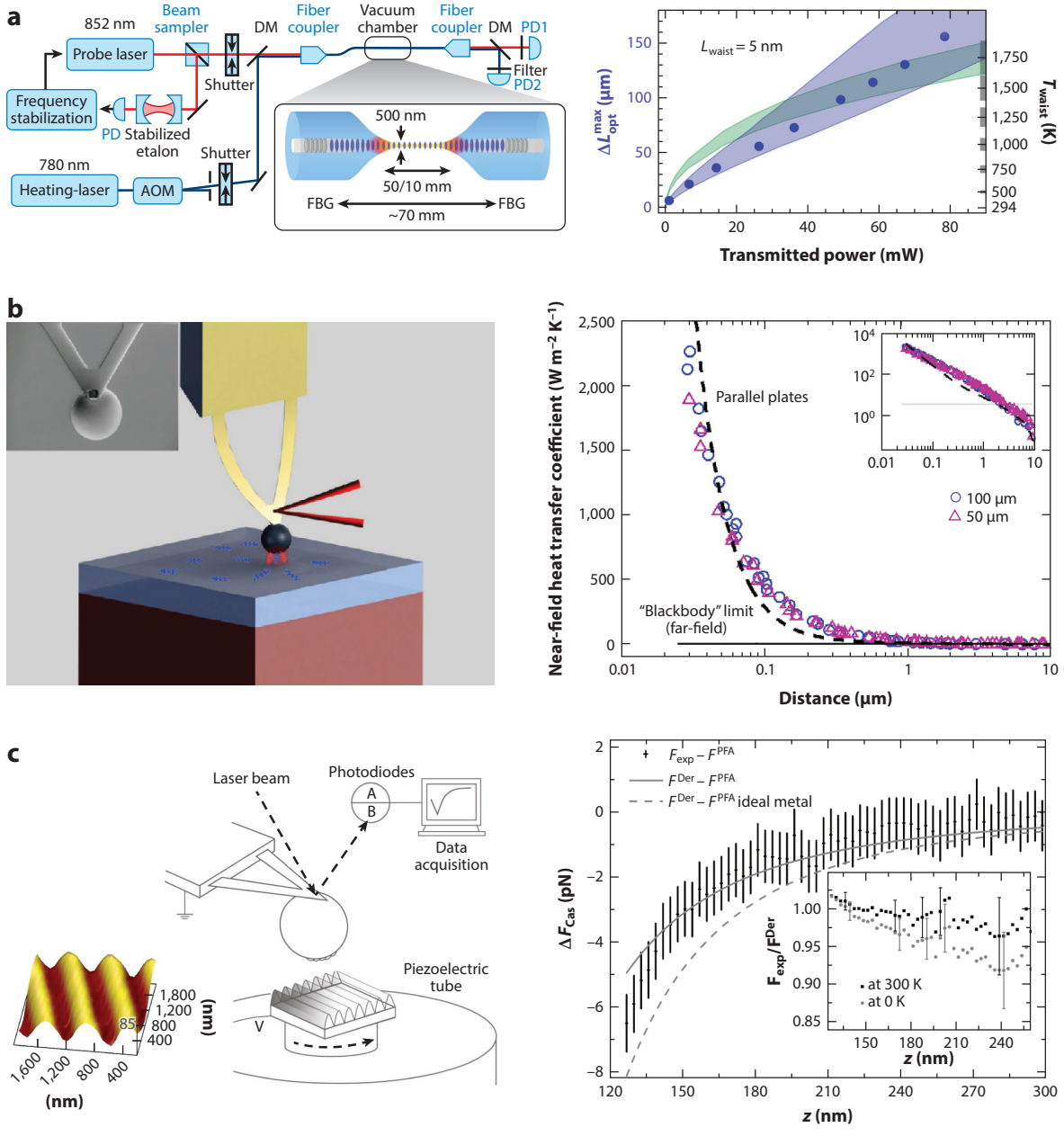

Figure 1

(*a*) Thermal radiation from a silica nanofiber (diameter 500 nm) from Reference 18, measured through cooling rates of the fiber; green bands are predictions from Planck's law, purple bands from Equation 38. The width of the bands reflects uncertainty in the fiber's dielectric properties. Adapted from Reference 18 with permission. (*b*) Heat transfer from a heated glass bead (blue circles and violet triangles refer to diameters of 100 and 50 microns, respectively) to a flat glass surface (from Reference 19) exceeds the Stefan–Boltzmann law (*solid line*) by orders of magnitude at separations below 0.1 micron. Adapted from Reference 19 with permission. (*c*) The equilibrium Casimir force between a corrugated surface and a corrugated sphere (20) is well described by a corresponding theory (*solid line*). Adapted from Reference 20 with permission. Abbreviations: AOM, acousto-optic modulator; DM, dichroic mirror; FBG, fiber Bragg-grating; PD, photodiode; PFA, proximity force approximation.

Theoretical studies of these effects have been carried out for spheres, plates, and cylinders[2] with the scattering formalism (11, 21–27). Recent studies on superscattering properties of subwavelength nanostructures (e.g., nanorods) (28) make such systems potential candidates for efficient heat transfer applications.

Macroscopic bodies: Radiate proportional to their surface area

2. **Heat transfer** between multiple objects is further complicated by the appearance of another scale, their separation, yielding nontrivial effects if they are smaller or comparable with the thermal wavelength. Indeed, over 40 years ago Polder & van Hove used FE to predict that radiative heat transfer between objects separated by a vacuum gap can exceed the blackbody limit (29) due to evanescent EM fields decaying exponentially into the vacuum. After the pioneering experiments in the late 1960s and early 1970s (30, 31), the enhancement of heat transfer in the near-field regime (generally denoting separations small compared to the thermal wavelength) has only recently been conclusively verified experimentally (19, 32–37). The results of one such experiment are depicted in **Figure 1*b***. Theoretically, heat transfer has been considered for a limited number of shapes: parallel plates (9, 29, 38, 39), a dipole or sphere in front of a plate (24, 40, 41), two dipoles or spheres (40, 42, 43), and a cone in front of a plate (44). The scattering formalism has been successfully exploited (6, 11, 17, 24, 45–47) in these contexts, using powerful numerical techniques (44, 48, 49) for arbitrary geometries and analytical computations for planar, cylindrical, spherical, and ellipsoidal cases (50, 51).
3. **Casimir forces** in equilibrium have been the subject of considerable theoretical investigation and were finally confronted with several high-precision experiments in the 1990s (52–54). The interested reader is referred to the extensive literature on the subject, a sampling of which is in References 3 and 55–58. The bottom row of **Figure 1** depicts a recent example of Casimir force measurement between a corrugated surface and a corrugated sphere (20). Even for this complicated geometry, precise comparisons between theory and experiment are now possible. There have been comparatively few studies of the Casimir force between objects at different temperatures. The force due to radiation pressure at large distances is modified by near-field effects at separations less than the thermal wavelength. Nonequilibrium forces were theoretically predicted, initially between two plates or between a plate and an atom (13, 59, 60), and were later extended to other shapes with the scattering formalism (17, 45, 47). There has so far been only one experiment on the Casimir-Lifshitz force out of equilibrium (61) involving an ultracold atomic cloud at a distance of a few microns from a dielectric substrate. It is hoped that there will be further high-precision experiments of nonequilibrium forces between solid objects, and indeed there has been a proposal (62–65) to employ differential measurements (66, 67) to this end.

2. FLUCTUATIONAL ELECTRODYNAMICS

The goal of FE is to study the phenomena originating from fluctuations of the EM field in macroscopic (globally neutral) bodies, importantly in the near-field regime of small distances. A first-principle analysis starting from the known quantum mechanical interactions of the individual atoms comprising the two bodies is feasible only for rarefied objects. The microscopic approach

[2] Although the results are exact for plates and spheres, the radiation by a cylinder is obtained within certain approximations (21–23).

becomes unpractical for macroscopic bodies, owing to complicated inductive many-body effects that arise for particle densities characteristic of condensed matter. Indeed, for separations much larger than interatomic distances, a continuum description is appropriate, and interactions can be regarded as occurring through the always present fluctuating EM field in the interior of absorbing media as a result of the endless quantum and thermal motions of its constituent charges. This field is not simply confined to the interior of the bodies but stretches out well beyond, partly in the form of propagating waves and partly as exponentially decaying evanescent waves. Consequently, absorbing bodies are surrounded by an envelope of EM fluctuations. When two or more bodies are in close proximity, their EM envelopes overlap mediating energy or momentum transfer between them, even in the absence of direct physical contact. For computing interactions, the relevant wavelengths of the fluctuating EM field should be comparable with macroscopic scales and separation, and thus a description in terms of macroscopic EM features of the bodies should be feasible. The macroscopic approach outlined here has a large degree of generality: It naturally embodies thermal effects as well as retardation phenomena associated with the finite speed of light. As a check, the method should (and does) reproduce results obtained by considering quantum mechanical interactions of individual atoms, in the limit of dilute media.

To determine the statistical features of the EM field surrounding an absorbing body, Rytov (11, 68) postulated that the fluctuations are sourced by randomly fluctuating currents of density $\mathbf{j}(\mathbf{r}, t)$ in the interior of the body. Physically, the current $\mathbf{j}(\mathbf{r}, t)$ originates from the quantum and thermal random motions of the charges that constitute the body, i.e., conduction electrons in a conductor, bound electrons in a dielectric, or ions in a polar dielectric. The random field $\mathbf{j}(\mathbf{r}, t)$ is analogous to the random force in the theory of Brownian motion. Consistent with the macroscopic character of the theory, it is assumed that the EM field generated by the random current obeys the macroscopic classical Maxwell's equations, which for a monochromatic field (with time dependence proportional to $e^{-\mathrm{i}\omega t}$) in a dielectric, nonmagnetic inhomogeneous medium are

$$\nabla \times \mathbf{E}(\mathbf{r}, \omega) = \mathrm{i}\,\frac{\omega}{c}\,\mathbf{H}(\mathbf{r}, \omega), \tag{1}$$

$$\nabla \times \mathbf{H}(\mathbf{r}, \omega) = -\mathrm{i}\,\varepsilon(\mathbf{r}, \omega)\frac{\omega}{c}\mathbf{E}(\mathbf{r}, \omega) + \frac{4\pi}{c}\mathbf{j}(\mathbf{r}, \omega), \tag{2}$$

where $\varepsilon(\mathbf{r}, \omega)$ is the complex electric permittivity of the medium. The above equations hold in the interior of each body and must be supplemented with the usual boundary conditions on the fields $\mathbf{E}(\mathbf{r}, \omega)$ and $\mathbf{H}(\mathbf{r}, \omega)$ on the surfaces of the bodies. The presence of the random source $\mathbf{j}(\mathbf{r}, \omega)$ gives to Equation 2 the character of a Langevin equation for the EM field. The random current has zero mean, $\langle \mathbf{j}(\mathbf{r}, \omega) \rangle = 0$, and its statistical properties are described by its two-point correlation function, providing the (quantum and thermal) average of the product of components of $\mathbf{j}(\mathbf{r}, \omega)$ at two different points $\mathbf{r}$ and $\mathbf{r}'$ inside the body. By the very nature of the macroscopic approach, in which atomic distances are considered to be negligibly small, this correlation has the form of a delta function $\delta(\mathbf{r} - \mathbf{r}')$. Thus, following Rytov, the current correlator is

$$\left\langle j_i(\mathbf{r}, \omega) j_k^*(\mathbf{r}', \omega') \right\rangle = \frac{\hbar\omega^2}{2} \coth\left(\frac{\hbar\omega}{2k_B T}\right) \mathrm{Im}\,\varepsilon(\mathbf{r}, \omega)\delta_{ik}\delta(\mathbf{r} - \mathbf{r}')\delta(\omega - \omega'). \tag{3}$$

Here, i and k label vector components, and T is the temperature. Because in quantum theory the current density is an operator, the correlator is more precisely the average of the symmetrized product of the components of the current operator. Equation 3 is a form of the fluctuation dissipation theorem (69), relating fluctuations of the currents to the dissipative response of the system,

represented by the dielectric function $\varepsilon(\mathbf{r},\omega)$. The identity,

$$\frac{1}{2}\hbar\omega\coth\left(\frac{\hbar\omega}{2k_BT}\right)=\hbar\omega\left[\frac{1}{2}+\frac{1}{\exp(\hbar\omega/k_BT)-1}\right], \tag{4}$$

recasts the correlator in Equation 3 as the sum of a purely quantum contribution, represented by the first term between the brackets, and a thermal contribution that is proportional to the Bose-Einstein average occupation.

The EM field outside the body can be obtained by solving Maxwell Equation 2, with $\mathbf{j}(\mathbf{r},\omega)$ as a source, using the Green's function formalism: The dyadic Green's function $\mathcal{G}_{ik}(\omega;\mathbf{r},\mathbf{r}')$ gives the electric field $E_i(\mathbf{r},\omega)$ at point $\mathbf{r}$, generated by a point-like current source at the point $\mathbf{r}'$ inside the dielectric body. To preserve causality, $\mathcal{G}_{ik}(\omega;\mathbf{r},\mathbf{r}')$ is subjected to retarded boundary conditions. It is worth pointing out that the Green's function automatically takes into account nonadditive many-body effects associated with the induced currents caused by the presence of the point-like source at $\mathbf{r}'$. Using the Green's function, the electric field generated by the continuous distribution of currents is expressed as:

$$E_i(\mathbf{r},\omega)=\frac{4\pi\,\mathrm{i}\,\omega}{c^2}\int \mathrm{d}^3\mathbf{r}'\mathcal{G}_{ik}(\omega;\mathbf{r},\mathbf{r}')\,j_k(\mathbf{r}',\omega). \tag{5}$$

Of course, since the random current has zero mean, the average electric field vanishes. However, the observables of interest are quadratic in the field components. For example, the force acting on a body is obtained by integrating the Maxwell tensor T_{ij} over a closed surface drawn in the empty space outside the body and enclosing the body in its interior, whereas the radiated power received by the body is obtained by integrating over such a surface with the Poynting vector $\mathbf{S}$. The average value of any quadratic observable in the EM field can be computed starting from the correlator of the electric field $\langle E_i(\mathbf{r},t)E_j(\mathbf{r}',t')\rangle$ (the first Maxwell equation relates correlators involving the magnetic field to those from the electric field by suitable curl operations). It follows from Equations 3 and 5 that the Fourier transform of $\langle E_i(\mathbf{r},t)E_j(\mathbf{r}',t')\rangle$ does not vanish and has the expression

$$\begin{aligned}\left\langle E_i(\mathbf{r},\omega)E_j^*(\mathbf{r}',\omega')\right\rangle &= \frac{8\pi^2\hbar\omega^4}{c^4}\coth\left(\frac{\hbar\omega}{2k_BT}\right)\delta(\omega-\omega')\\ &\quad\times\int \mathrm{d}^3\mathbf{r}''\mathcal{G}_{ik}(\omega;\mathbf{r},\mathbf{r}'')\ \mathrm{Im}\ \varepsilon(\omega,\mathbf{r}'')\mathcal{G}_{kj}^*(\omega;\mathbf{r}'',\mathbf{r}').\end{aligned} \tag{6}$$

2.1. Systems in Global Thermal Equilibrium

When the system is in global thermal equilibrium at a temperature T, the integral over space on the right-hand side of Equation 6 can be expressed in terms of the imaginary part of the Green's function, using the important identity

$$\frac{\omega^2}{c^2}\int \mathrm{d}^3\mathbf{r}''\mathcal{G}_{ik}(\omega;\mathbf{r},\mathbf{r}'')\ \mathrm{Im}\ \varepsilon(\omega,\mathbf{r}'')\mathcal{G}_{kj}^*(\omega;\mathbf{r}'',\mathbf{r}')=\mathrm{Im}\ \mathcal{G}_{ij}(\omega;\mathbf{r},\mathbf{r}'). \tag{7}$$

Inserting the above relation into the right-hand side of Equation 6 leads to

$$\left\langle E_i(\mathbf{r},\omega)E_j^*(\mathbf{r}',\omega')\right\rangle=\frac{8\pi^2\hbar\omega^2}{c^2}\coth\left(\frac{\hbar\omega}{2k_BT}\right)\delta(\omega-\omega')\ \mathrm{Im}\ \mathcal{G}_{ij}(\omega;\mathbf{r},\mathbf{r}'). \tag{8}$$

Equation 8 is remarkable, indicating that in thermal equilibrium the correlator of the electric field at points outside the bodies is determined solely from knowledge of the Green's function in their exterior. Indeed, it has been shown (70, 71) that Equation 8 can be directly obtained from

the fluctuation-dissipation theorem by regarding the Green's function itself as a response of the system to external sources outside the bodies, without resorting to hypothetical random currents in their interior. Another important feature of the equilibrium is that the retarded Green's function of a passive medium is analytical in the upper complex frequency plane (72). By virtue of this analyticity, the equal-time correlator of the electric field $\langle E_i(\mathbf{r},t)E_j(\mathbf{r}',t)\rangle$ can be expressed, after a Wick-rotation of the frequency axis, as a sum over the imaginary poles $\omega_n = 2\pi i n k_B T/\hbar \equiv i\xi_n$, for $n = 0, 1, \ldots$ (the so-called Matsubara frequencies) of the hyperbolic cotangent in Equation 8:

$$\langle E_i(\mathbf{r},t)E_j(\mathbf{r}',t)\rangle = \frac{8\pi k_B T}{c^2} {\sum_n}' \xi_n^2 \mathcal{G}_{ij}(i\xi_n;\mathbf{r},\mathbf{r}'), \tag{9}$$

where the prime implies that the $n = 0$ term has to be taken with weight 1/2. As Green's functions are much better behaved along the imaginary axis than along the real frequency axis, Equation 9 is considerably easier to estimate numerically in practical applications.

Equation 8 shows how the spectral density of the fluctuating EM field is modified by the presence of one or more bodies, and in principle it allows determination of the fluctuation of the electric field for any number of dielectric bodies of any shape in global thermal equilibrium. The difficulty resides of course in the computation of the Green's function $\mathcal{G}_{ij}(\omega;\mathbf{r},\mathbf{r}')$. For simple geometries and/or arrangements of the bodies, the Green's function can be found analytically, but in general its computation is hard and can be only achieved numerically. An important conclusion about the influence of material properties on equilibrium field correlators, and hence the observables computed from them, can be deduced from the imaginary-frequency formula in Equation 9: Since the electric permittivity $\varepsilon(i\xi)$ of all causal materials is positive and monotonically decreasing along the imaginary frequency (72), equilibrium values of field correlators are substantially insensitive to the structure of the resonances that the dielectric function may display for real frequencies.

The simplest situation is that of an infinite homogeneous dielectric medium (72). The Green's function $\mathcal{G}_{ij}^{(0)}(\omega;\mathbf{r},\mathbf{r}')$ in this case is known analytically, and the correlators of the EM field can be obtained in closed form. In the limit of a transparent medium, corresponding to $\mathrm{Im}\,\varepsilon \to 0$ (with $\mathrm{Re}\,\varepsilon > 0$), it is possible to verify that the spectral decomposition of the EM energy density computed with Equation 8 reproduces, after subtraction of the unphysical contribution of zero-point fluctuations, the spectral decomposition of the blackbody radiation in a transparent medium. In confined geometries, Equation 8 can be used to study how the blackbody spectrum is modified by the shape and material properties of the cavity walls, influencing the spectral lines and lifetimes of atoms placed inside the cavity (70).

An important application of the equilibrium formulae in Equations 8 and 9 is to the Casimir effect (4). This is the force between two neutral macroscopic polarizable bodies that originates from quantum and thermal fluctuations of the EM field in the region of space bounded by the surfaces of the two bodies. As one of the rare manifestations of quantum mechanics at the macroscopic domain, like superconductivity or superfluidity, this force has attracted considerable interest, also in view of its potential applications to nanotechnology, condensed matter physics, gravitation, and cosmology (see, e.g., reviews in References 3, 12, 55, 56, 58). In his seminal work Casimir computed the force F_C between two neutral perfectly conducting plane parallel plates of area A at a distance d in vacuum; by carefully summing the zero-point energies of the EM modes in the empty space between them, he found

$$F_C = \frac{\pi^2 \hbar c}{240} \frac{A}{d^4}. \tag{10}$$

The presence of Planck's constant clearly points to the quantum origin of the Casimir force. In the framework of FE the Casimir force is estimated by integrating the Maxwell stress tensor across a closed surface S drawn in a vacuum and surrounding one of the two bodies. This in turn involves evaluating an integral on S of field correlators evaluated at coinciding points $\mathbf{r} = \mathbf{r}'$ along S. Because the field correlators diverge at coincidence points, as the Green's function $\mathbf{G}(\omega; \mathbf{r}, \mathbf{r}')$ diverges in such limit, it is not immediately clear if a well-defined force can be obtained. That this is indeed so is recognized by considering the following decomposition of the Green's function at points outside the bodies:

$$\mathcal{G}_{ij}(\omega; \mathbf{r}, \mathbf{r}') = \mathcal{G}_{ij}^{(0)}(\omega; \mathbf{r}, \mathbf{r}') + \mathcal{G}_{ij}^{(\text{bodies})}(\omega; \mathbf{r}, \mathbf{r}'), \tag{11}$$

where as before $\mathcal{G}_{ij}^{(0)}(\omega; \mathbf{r}, \mathbf{r}')$ represents the free Green's function in infinite space, and $\mathcal{G}_{ij}^{(\text{bodies})}(\omega; \mathbf{r}, \mathbf{r}')$ is the contribution due to the presence of the bodies. In the coincidence limit $\mathbf{r} \to \mathbf{r}'$, only the free space Green's function diverges, whereas the body Green's function $\mathcal{G}_{ij}^{(\text{bodies})}(\omega; \mathbf{r}, \mathbf{r}')$ attains a finite limit (17). It is clear physically that the ill-defined contribution to the stress tensor originating from the free-space Green's function, being independent of the positions and material properties of the bodies, can be disregarded altogether, and that the Casimir force is determined solely by the well-defined stresses associated with the body Green's function. A computation of the Casimir force along these lines was first performed by Lifshitz (5) for the case of two plane-parallel semi-infinite dielectric slabs. In this simple geometry, the body Green's function $\mathcal{G}_{ij}^{(\text{bodies})}(\omega; \mathbf{r}, \mathbf{r}')$ can be easily determined analytically by working in a basis of plane waves propagating in the plane of the slab surfaces (17), and it can be expressed in terms of the Fresnel reflection coefficients of the slabs (73). Lifshitz's formula enables computing the influence of real material properties of the bounding plates, like their finite reflectivity and temperature, and is routinely used today to interpret modern precision measurements of the Casimir force.

A major unresolved problem in Casimir physics concerns the magnitude of the thermal contribution to the Casimir force between two conducting plates. In essence the puzzle is about the role played by relaxation properties of conduction electrons in the Lifshitz theory (56, 74). It turns out that Lifshitz's formula predicts significantly different magnitudes for the thermal force depending on whether the optical data of the conductor are extrapolated toward zero frequency on the basis of the Drude model (which does take dissipation into account) or instead by the dissipationless plasma model of IR optics. In addition to predicting different magnitudes for the thermal force, it has been shown that the two prescriptions have important thermodynamic consequences: Although the Drude prescription leads to a violation of Nernst heat theorem (in the idealized case of two conducting plates with a perfect crystal structure) (75), the plasma prescription violates the Bohr-van Leeuwen theorem of classical statistical physics (76, 77). It has been suggested in Reference 78 that the reported violation of the Nernst heat theorem by Drude metals may be due to a glassy state of quasi-static Foucault currents in Drude metals at low temperatures, rendering the Nernst theorem inapplicable. The experimental situation is contradictory: Although several small-distance experiments (79–81) probing separations below one micron appear to be in agreement with the plasma model and to rule out the larger thermal force predicted by the Drude model, a recent large-distance experiment in the wide range from 0.7 to 7.3 μm (82) has been interpreted as being in agreement with the Drude model. A novel experimental scheme based on differential Casimir force measurements (62–64) may lead to a definitive clarification of the problem. A very recent experiment (66, 67) based on this scheme, utilizing samples with alternating Au-Ni regions, appears to be very encouraging.

2.2. Systems Out of Thermal Equilbrium

For out of equilibrium situations in which we can assign to each body (in its rest frame) a distinct temperature T, the basic assumption of FE (11, 68) is that current fluctuations in each body still satisfy Equation 3. Electric field fluctuations outside the bodies are obtained by summing contributions from the different objects, generalizing Equation 6. The technical difficulty is in expressing the Green's function for the collection of bodies, in terms of their individual Green's functions. We note that when studying problems of heat transfer, the contribution of vacuum quantum fluctuations (corresponding to the first term on the right-hand side of Equation 4) can be ignored altogether because, being independent of the bodies' temperatures, vacuum fluctuations contribute nothing to energy transfers.

The problem of radiative heat transfer for two plane-parallel homogeneous dielectric slabs at (arbitrary) different temperatures was first studied by Polder & van Hove, using Rytov theory (29), extending a previous investigation by Rytov of the less realistic case of a heated dielectric slab facing an almost perfect mirror at zero temperature (11). The main finding of Polder & van Hove is the strong increase of radiative heat transfer between two metallic surfaces for gap widths smaller than the characteristic thermal wavelength $\lambda_T = \hbar c/(2\pi k_B T)$ ($\lambda_T = 1.2$ μm at room temperature). Subsequent studies by other authors (83) revealed that near-field radiative heat transfer can in fact be enhanced by several orders of magnitude when the surfaces are covered by adsorbates or can support low-frequency surface plasmons, via a mechanism of resonant photon tunneling. The strong increase of the power of radiative transfer at the nanoscale opens up the possibility of important technological applications including heat-assisted magnetic recording (85), near-field thermophotovoltaics (86), and lithography (9).

Rytov theory out of thermal equilibrium has been recently used to investigate the Casimir force between two dielectric slabs at different temperatures in vacuum (13). Out of thermal equilibrium the Casimir-Lifshitz force displays remarkable features that disappear when the system is brought to a state of thermal equilibrium. These features originate from a peculiar contribution, $\bar{F}^{(\mathrm{neq})}(T_1, T_2)$, to the nonequilibrium force, which is antisymmetric under an exchange of temperatures T_1 and T_2. Being antisymmetric in the body temperatures, this term can have either sign and can in principle be harnessed to tune the force both in strength and sign (87) and to realize self-propelling systems (6) (see Section 5).

3. SCATTERING THEORY

As discussed above, various fluctuation-induced effects can be described within Rytov's theory as emerging from fluctuating, random currents inside the bodies. The correlation functions of these currents is then related by the Green's function to the corresponding fields from which the relevant observables such as forces and energy fluxes are obtained. Hence, it is desirable to express the energy of a system of bodies such that each carries a prescribed charge and current distribution in terms of these quantities. With this functional, one can then average over random currents to obtain the free energy or field correlation functions. As we described below, the answer to this is given by scattering theory.

Before we describe the general scattering approach, it is instructive to look at the energy of two distant conductors of arbitrary shape. Putting a charge on one conductor changes the potential of the other by an amount that depends on the geometrical configuration and the individual capacitances of the conductors. The potential m_{12} to which conductor 2 is raised when a unit charge is placed on conductor 1 is known as elastance. Due to Green's reciprocity theorem, one has $m_{12} = m_{21}$ so that the elastance matrix $M = [m_{\alpha\beta}]$ is symmetric. Because the potentials of the

conductors are given by $[V_1, V_2] = M\,[Q_1, Q_2]$ in terms of their charges, the electrostatic energy has the quadratic form $E = \frac{1}{2}[Q_1, Q_2]^t M\,[Q_1, Q_2]$. We shall see below that a similar quadratic form is obtained for the energy of a system of arbitrarily shaped dielectric bodies with (frequency-dependent) fluctuating currents.

The elastance matrix contains information about the shapes and relative positions of the objects. Let the two conductors have capacitances C_1 and C_2 in isolation. When 1 is uncharged, and 2 with charge Q_2 is placed at a distance d (which is assumed to be much larger than the linear dimension R of the conductors), the potential of 1 is raised to $Q_2/(4\pi d)$; hence $m_{21} = 1/(4\pi d)$. On the nearer half of 1 a charge of opposite sign to Q_2 and of magnitude $C_1 Q_2/(4\pi d) \sim Q_2 R/d$ is induced (and an equal charge of equal sign is induced on the remote half). This leads at 2 to a dipole potential of the order $Q_2 R^2/d^3$ that can be ignored to leading order in R/d. Hence the potential V_2 is not affected by 1, and we obtain $m_{22} = V_2/Q_2 = C_2^{-1}$, and similar for m_{11}, such that the elastance matrix is

$$M = \begin{bmatrix} C_1^{-1} & (4\pi d)^{-1} \\ (4\pi d)^{-1} & C_2^{-1} \end{bmatrix}. \tag{12}$$

Note that the self- and mutual capacitances are given by the inverse of the matrix M. This matrix shows two interesting features. The diagonal elements contain solely information about the shape of the objects (via their capacitances), whereas the off-diagonal elements depend only on their relative position.

Now consider the general situation of arbitrarily shaped dielectric bodies that carry fluctuating currents $\mathbf{J}_j(\omega)$ where j numbers the bodies and ω is the frequency. The equivalent of the capacitance is the scattering amplitude, also known as the $\mathbb{T}$ operator (88). It quantifies the fluctuating currents induced on a body in response to an incident EM field. We briefly review the key results from scattering theory: The general solution of the wave equation

$$[\mathbb{H}_0 - \mathbb{V}(\omega, \mathbf{x})]\mathbf{E}(\omega, \mathbf{x}) = \frac{\omega^2}{c^2}\mathbf{E}(\omega, \mathbf{x}), \tag{13}$$

with differential and potential operators

$$\mathbb{H}_0 = \boldsymbol{\nabla} \times \boldsymbol{\nabla} \times, \tag{14}$$

$$\mathbb{V}(\omega, \mathbf{x}) = -\mathbb{I}\frac{\omega^2}{c^2}[1 - \epsilon(\omega, \mathbf{x})] - \boldsymbol{\nabla} \times \left[\frac{1}{\mu(\omega, \mathrm{x})} - 1\right]\boldsymbol{\nabla} \times, \tag{15}$$

is given by the Lippmann-Schwinger equation

$$\mathbf{E} = \mathbf{E}_0 + \mathbb{G}_0 \mathbb{V}\mathbf{E}. \tag{16}$$

Here $\mathbb{G}_0$ is the free EM tensor Green's function, and the homogeneous solution $\mathbf{E}_0$ obeys the wave equation with $\mathbb{V} = 0$. Iterative substitution for $\mathbf{E}$ in Equation 16 leads to

$$\mathbf{E} = \mathbf{E}_0 + \mathbb{G}_0 \mathbb{V}\mathbf{E}_0 + \mathbb{G}_0 \mathbb{V}\mathbb{G}_0 \mathbb{V}\mathbf{E} - \ldots \equiv \mathbf{E}_0 + \mathbb{G}_0 \mathbb{T}\mathbf{E}_0, \tag{17}$$

where the $\mathbb{T}$ operator is defined as

$$\mathbb{T} = \mathbb{V}\frac{\mathbb{I}}{\mathbb{I} - \mathbb{G}_0 \mathbb{V}} = \mathbb{V}\mathbb{G}\mathbb{G}_0^{-1}, \tag{18}$$

and $\mathbb{G}$ is the Green's function of the wave equation in Equation 13, given explicitly by

$$\mathbb{G} = \mathbb{G}_0 + \mathbb{G}_0 \mathbb{T}\mathbb{G}_0. \tag{19}$$

We note that $\mathbb{T}$, $\mathbb{G}_0$, and $\mathbb{G}$ are all functions of frequency ω and nonlocal in space. As can be seen from expanding $\mathbb{T}$ in Equation 18 in a power series, $\mathbb{T}(\omega, \mathbf{x}, \mathbf{x}') = \langle \mathbf{x}|\mathbb{T}(\omega)|\mathbf{x}'\rangle$ is zero whenever $\mathbf{x}$ or $\mathbf{x}'$ are not located on an object, i.e., where $\mathbb{V}(\omega, \mathbf{x})$ is zero.

The matrix elements of the $\mathbb{T}$ operator are given by the scattering amplitude $\mathcal{T}$ in a given basis, e.g., vector spherical waves. We consider a scattering process in which a regular wave $\mathbf{E}_\alpha^{\mathrm{reg}}$ interacts with a body and scatters outward in the form of an outgoing wave $\mathbf{E}_\beta^{\mathrm{out}}$. Here α and β label basis elements. We choose a convenient "scattering origin" inside the body, consistent with any symmetries of the problem if possible.

To find the field $\mathbf{E}$ at a coordinate $\mathbf{x}$ far enough outside the body, we employ Equation 17 in position space and the usual expansion of $\mathbb{G}_0$ in terms of regular and outgoing waves,

$$\mathbf{E}(\omega, \mathbf{x}) = \mathbf{E}_\alpha^{\mathrm{reg}}(\omega, \mathbf{x}) + \sum_\beta \mathbf{E}_\beta^{\mathrm{out}}(\omega, \mathbf{x})\mathcal{T}_{\beta\alpha}(\omega), \tag{20}$$

where the scattering amplitude is defined by

$$\mathcal{T}_{\beta\alpha}(\omega) = i \iint \mathbf{E}_\beta^{\mathrm{reg}*}(\omega, \mathbf{x}') \cdot \mathbb{T}(\omega, \mathbf{x}', \mathbf{x}'')\mathbf{E}_\alpha^{\mathrm{reg}}(\omega, \mathbf{x}'')\mathrm{d}\mathbf{x}'\mathrm{d}\mathbf{x}''. \tag{21}$$

In analogy to the electrostatic case in Equation 12, we can now express the kernel of the action for the fluctuating currents at fixed frequency on an arbitrary number of bodies,

$$S(\omega) = \frac{1}{2}\mathbf{J}_j\mathbb{M}_{jk}\mathbf{J}_k, \tag{22}$$

in terms of the inverse of the $\mathbb{T}$ operators $\mathbb{T}_j$ of the individual bodies, replacing the inverse capacitances on the diagonal,

$$\mathbb{M} = \begin{bmatrix} -\mathbb{T}_1^{-1} & \mathbb{U}^{12} & \mathbb{U}^{13} & \cdots \\ \mathbb{U}^{21} & -\mathbb{T}_2^{-1} & \mathbb{U}^{23} & \cdots \\ \cdots & \cdots & \cdots & \cdots \end{bmatrix}. \tag{23}$$

In analogy to the electrostatic case, the off-diagonal operators of this kernel describe the interaction of the currents on different objects. Hence, the operators $\mathbb{U}^{\alpha\beta}$ must be related to the free Green's function $\mathbb{G}_0$. The latter can be expanded as

$$\mathbb{G}_0(\omega, \mathbf{x}, \mathbf{x}') = i \sum_\alpha \begin{cases} \mathbf{E}_\alpha^{\mathrm{out}}(\omega, \xi_1, \xi_2, \xi_3) \otimes \mathbf{E}_\alpha^{\mathrm{reg}*}(\omega, \xi_1', \xi_2', \xi_3') & \text{if } \xi_1(\mathbf{x}) > \xi_1'(\mathbf{x}') \\ \mathbf{E}_\alpha^{\mathrm{reg}*}(\omega, \xi_1, \xi_2, \xi_3) \otimes \mathbf{E}_\alpha^{\mathrm{out}}(\omega, \xi_1', \xi_2', \xi_3') & \text{if } \xi_1(\mathbf{x}) < \xi_1'(\mathbf{x}') \end{cases}, \tag{24}$$

where one of the spatial coordinates is identified as the "radial" variable and treated differently from the remaining coordinates. We let ξ_1 represent this coordinate and denote the remaining coordinates as ξ_2 and ξ_3. We introduce the "outgoing" solution in ξ_1, which is in the same scattering channel as the corresponding regular solution but obeys outgoing wave boundary conditions as $\xi_1 \to \infty$. It is linearly independent of the regular solution. Because the $\mathbb{T}$ operators for the individual bodies in Equation 23 are defined relative to the basis appropriate for each body, one has to translate the scattering solution of one body to the basis of the other body. We assume that all objects are placed outside of each other (see **Figure 2*b***). The outgoing solutions form a complete set independent of the origin used to define the decomposition into a basis of partial waves. Let $\{\mathbf{E}_\beta^{\mathrm{reg}}(\omega, \mathbf{x}_j)\}$ be the regular solutions expressed with respect to the origin of coordinates appropriate to object j, $\mathcal{O}_j$. Except in a region that contains the origin $\mathcal{O}_i$, where $\mathbf{E}_\alpha^{\mathrm{out}}(\omega, \mathbf{x}_i)$ is singular, one can expand an outgoing solution in terms of the

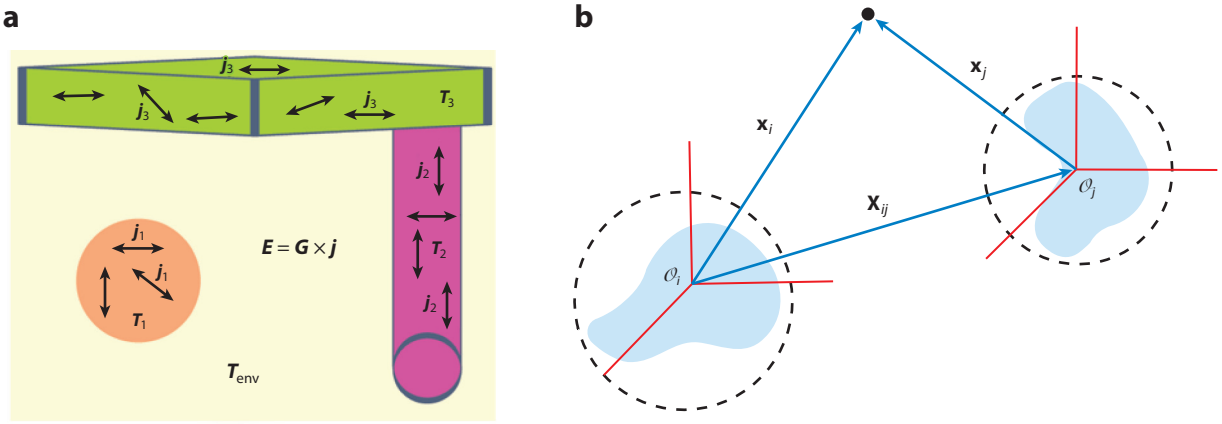

Figure 2

(*a*) Fluctuations of the electromagnetic (EM) field outside several bodies, sourced by the fluctuating currents in each body. (*b*) Geometry of the configuration of two objects as introduced in Section 3. The dotted lines show surfaces separating the objects on which the radial variable is constant. The translation vector $\mathbf{X}_{ij} = \mathbf{x}_i - \mathbf{x}_j = -\mathbf{X}_{ji}$ describes the relative positions of the two origins. Although the operator formalism is completely general, applicable to any configuration, for objects enclosed by nonoverlapping spheres or ellipsoids a representation in partial waves is possible.

$$\{\mathbf{E}^{\mathrm{reg}}_{\beta}(\omega, \mathbf{x}_j)\},$$

$$\mathbf{E}^{\mathrm{out}}_{\alpha}(\omega, \mathbf{x}_i) = \sum_{\beta} \mathbb{U}^{ji}_{\beta\alpha}(\omega, \mathbf{X}_{ji}) \mathbf{E}^{\mathrm{reg}}_{\beta}(\omega, \mathbf{x}_j), \text{ for } \mathbf{x} \notin N(\mathcal{O}_i), \tag{25}$$

where $\mathbf{X}_{ij} = -\mathbf{X}_{ji} = \mathbf{x}_i - \mathbf{x}_j$ is shown in **Figure 2*b***. Note that $\mathbf{x}_i$ and $\mathbf{x}_j$ refer to the same position in space, $\mathbf{x}$, expressed as the displacement from different origins. Here $N(\mathcal{O}_i)$ is a neighborhood of the origin $\mathcal{O}_i$. This expansion defines the matrix elements of the operator $\mathbb{U}_{\beta\alpha}$ in a given basis. We note that while the operator formalism in terms of $\mathbb{G}_0$ and $\mathbb{T}$ is fully general, expansion in partial waves imposes constraints on the relative position of the bodies, see **Figure 2*b***. There must exist an origin, and a separable coordinate system, so that for all points $\mathbf{x}$ in one object and $\mathbf{x}'$ in another, $\xi_1(\mathbf{x})$ is always greater than $\xi_1(\mathbf{x}')$, and vice versa. Having $\xi_1(\mathbf{x}) > \xi_1(\mathbf{x}')$ ensures that the Green's function is always evaluated by letting $\mathbf{x}$ be the argument of the outgoing wave function and $\mathbf{x}'$ that of the regular wave function. Therefore, any two objects must be separated by a surface defined by the locations $\mathbf{x}$ where $\xi_1(\mathbf{x})$ is constant.

This completes the construction of the kernel $\mathbb{M}$ which can be viewed in a given basis as the interaction matrix between multipole moments on the bodies. For a similar, earlier approach based on a multipole expansion for specific shapes like spheres and cylinders see Reference 89. With this energy functional for the fluctuating currents on a set of arbitrarily shaped dielectric objects, the free energy and field correlation functions of the system can be computed by averaging over the currents with the corresponding Boltzmann weight. The first application of this approach has been the computation of equilibrium Casimir interaction (14, 16). The Casimir energy can be written as

$$\mathcal{E}_0 = -\frac{\hbar c}{2\pi} \int_0^{\infty} \mathrm{d}\kappa \, \log Z(\kappa), \tag{26}$$

where we have Wick rotated from real to the imaginary frequencies κ, and $Z(\kappa)$ is the partition function for the action of Equation 22 for currents. After integrating over the currents, we

obtain

$$\mathcal{E} = \frac{\hbar c}{2\pi} \int_0^\infty \mathrm{d}\kappa \log\det(\mathbb{M}\mathbb{M}_\infty^{-1}), \tag{27}$$

where $\mathbb{M}_\infty^{-1}$ is a block diagonal matrix $\mathrm{diag}(\mathbb{T}_1\mathbb{T}_2\cdots)$. For two objects, the expression simplifies to

$$\mathcal{E} = \frac{\hbar c}{2\pi} \int_0^\infty \mathrm{d}\kappa \log\det\left(\mathbb{I} - \mathbb{T}_1\mathbb{U}^{12}\mathbb{T}_2\mathbb{U}^{21}\right). \tag{28}$$

At nonzero temperature T, the integral $\frac{\hbar c}{2\pi}\int_0^\infty d\kappa$ is replaced by $k_B T \sum_n'$, where $\kappa_n = \frac{2\pi n k_B T}{\hbar c}$ with $n = 0, 1, 2, 3\ldots$ is the nth Matsubara frequency. Careful analysis shows that the zero frequency mode is weighted by 1/2 compared to the rest of the terms in the sum; this modification of the sum is denoted by a prime on the summation symbol.

The scattering approach presented here builds on a range of previous related work: Scattering methods were first applied in the parallel plate geometry (73, 90–92), and within a multiple scattering approach for perfect mirrors of arbitrary shape at large separations (93, 94). The Krein formula for the density of states has also been employed to relate Casimir interactions to scattering data (95–102). Closely related path integral methods have been introduced for EM and scalar Casimir interactions (103–109). Recent progress became practically possible by the introduction of $\mathbb{T}$-operator-based approaches (110–112), which is closely related to Schwinger's view of Casimir forces in terms of current fluctuations (113) with many applications (114–119). More recently, fully numerical schemes have been shown to be powerful (44, 48, 49), as has a gradient expansion (120–122) yielding curvature corrections to the proximity force approximation (123) (**Figure 1**).

4. MERGING RYTOV AND SCATTERING THEORY

Having set out the elements of scattering theory, in this section we describe how it can be merged with the Rytov formalism to obtain heat radiation, heat transfer, and (Casimir) interactions for a set of arbitrary bodies in thermal nonequilibrium. We assume that N dielectric objects, labeled by $\alpha = 1, \ldots, N$, kept at time-independent, homogeneous temperatures $\{\mathbb{T}_\alpha\}$, are placed into an environment (vacuum) at temperature T_{env}. The bodies are characterized by their electric and magnetic response, $\epsilon(\omega; \mathbf{r}, \mathbf{r}')$ and $\mu(\omega; \mathbf{r}, \mathbf{r}')$, respectively, which can in general be nonlocal complex tensors, $\epsilon(\omega; \mathbf{r}, \mathbf{r}') = \varepsilon_{ij}(\omega; \mathbf{r}, \mathbf{r}')$, depending on frequency ω. In this nonequilibrium stationary state, each object is assumed to be at local equilibrium, such that current fluctuations locally satisfy the fluctuation dissipation condition. The general results for heat radiation, transfer, and force are given by the formulae in the sidebar Trace Formulas. We give below a compact derivation of these results; the interested reader is referred to Reference 17 for a detailed exposition.

In equilibrium, interactions (forces and torques) between objects can be obtained from the dependence on position and orientation of the free energy. There is no corresponding free energy for computation of nonequilibrium quantities like heat radiation and transfer. Instead, the correlation function $\mathbb{C}(\mathbf{r}, \mathbf{r}') = [\langle E_i(\mathbf{r}) E_j^*(\mathbf{r}')\rangle_\omega]_{i,j=1,2,3}$ is needed to compute the current-averaged components of the Maxwell tensor. We shall see below that even out of equilibrium $\mathbb{C}(\mathbf{r}, \mathbf{r}')$ is a superposition of equilibrium correlation functions, each at the temperature of the body that generates the corresponding contribution to the total field.

In equilibrium, the field correlations can be expressed as the superposition

$$\mathbb{C}^{\mathrm{eq}}(T) = a_0 \,\mathrm{Im}\,\mathbb{G} + \sum_\alpha \mathbb{C}_\alpha^{\mathrm{sc}}(T) + \mathbb{C}^{\mathrm{env}}(T), \tag{29}$$

with $a_0 \equiv \mathrm{sgn}(\omega)\frac{4\pi\hbar\omega^2}{2c^2}$. Here the first term represents the zero-point fluctuations, the sum in the second term is the radiation coming from the fluctuating sources inside the bodies, and the last term is the contribution of the environment,

$$\mathbb{C}^{\mathrm{env}}(T) = -a(T)\mathbb{G}\,\mathrm{Im}\left[\mathbb{G}_0^{-1}\right]\mathbb{G}^*, \tag{30}$$

with

$$a(T) \equiv \mathrm{sgn}(\omega)\frac{8\pi\hbar\omega^2}{c^2}[\exp(\hbar|\omega|/k_B T) - 1]^{-1}, \tag{31}$$

containing the occupation number of modes with frequency ω. In general, $\mathbb{C}_\alpha^{sc}(T)$ depends on all objects because the field radiated by body α is scattered by all other bodies. For the moment, we consider a single body at temperature T in a cold environment and neglect zero-point fluctuations. Using the scattering formalism, the correlations of the radiated field can be expressed in terms of the free Green's function and the body's T matrix $\mathbb{T}$, as

$$\mathbb{C}_\alpha^{\mathrm{sc,iso}}(T) = a(T)\mathbb{G}_0\left[\frac{i}{2}(\mathbb{T}^* - \mathbb{T}) - \mathbb{T}\,\mathrm{Im}(\mathbb{G}_0)\mathbb{T}^*\right]\mathbb{G}_0^*. \tag{32}$$

In the presence of additional objects, the Lippmann-Schwinger equation relates the total field $\mathbf{E}_\alpha$ to the field $\mathbf{E}_{\alpha,\mathrm{iso}}$ of object α alone by $\mathbf{E}_\alpha = \mathbb{O}_\alpha\mathbf{E}_{\alpha,\mathrm{iso}}$, with the multiple scattering operator

$$\mathbb{O}_\alpha = (1 + \mathbb{G}_0\mathbb{T}_{\tilde{\alpha}})\frac{1}{1 - \mathbb{G}_0\mathbb{T}_\alpha\mathbb{G}_0\mathbb{T}_{\tilde{\alpha}}}, \tag{33}$$

that depends also on the $\mathbb{T}$-operator $\mathbb{T}_{\tilde{\alpha}}$ of all other bodies. The final result for the multi-body correlation function $\mathbb{C}_\alpha^{\mathrm{sc}}(T)$ in Equation 29 is then given by

$$\mathbb{C}_\alpha^{\mathrm{sc}}(\mathbb{T}_\alpha) = \mathbb{O}_\alpha\,\mathbb{C}_\alpha^{\mathrm{sc,iso}}(\mathbb{T}_\alpha)\,\mathbb{O}_\alpha^\dagger. \tag{34}$$

We can thus express the full correlation function in terms of the free Green's function and the $\mathbb{T}$ operators. We can further eliminate the environment contribution and obtain the correlation function as a superposition of the radiation from the bodies at different temperatures $\mathbb{T}_\alpha$ as

$$\mathbb{C}^{\mathrm{neq}}[(\mathbb{T}_\alpha), T_{\mathrm{env}}] = \mathbb{C}^{\mathrm{eq}}(T_{\mathrm{env}}) + \sum_\alpha\left[\mathbb{C}_\alpha^{\mathrm{sc}}(\mathbb{T}_\alpha) - \mathbb{C}_\alpha^{\mathrm{sc}}(T_{\mathrm{env}})\right]. \tag{35}$$

With the functions expressed in terms of the $\mathbb{T}$ operators, we can compute radiated heat and forces. The heat H emitted by a body is obtained by integrating the normal component of the Poynting vector $\mathbf{S}$ over a surface Σ enclosing the body,

$$H = \oint_\Sigma \mathbf{S}\cdot\mathbf{n}, \tag{36}$$

with $\mathbf{S}(\mathbf{r}) = \frac{c}{4\pi}\int_{-\infty}^{\infty}\frac{\mathrm{d}\omega}{2\pi}\left\langle\mathbf{E}(\mathbf{r})\times\mathbf{B}^*(\mathbf{r})\right\rangle_\omega$. Note that forces on two bodies at different temperatures are no longer equal and opposite. The force on object α is found from the surface normal component of the stress tensor σ, integrated over a surface enclosing object α, as

$$\mathbf{F}^{(\alpha)} = \mathrm{Re}\oint_{\Sigma_\alpha}\sigma\cdot\mathbf{n}, \tag{37}$$

with $\sigma_{ij} = \int_{-\infty}^{\infty}\frac{\mathrm{d}\omega}{8\pi^2}\left\langle E_i E_j^* + B_i B_j^* - \frac{1}{2}\left(|E|^2 + |B|^2\right)\delta_{ij}\right\rangle_\omega$.

The above basis-independent operator expressions hold for any geometry. For practical computations, the operators have to be represented in a basis of partial waves. The traces of operators then turn into sums over matrix elements with respect to the partial wave indices. In the sidebar Trace Formulas, we present the general trace formulas for heat radiation, heat transfer, and forces both in the operator formalism and a basis of spherical vector waves (17). Note that in the latter case, the spheres enclosing the bodies cannot overlap (see also **Figure 2*b***).

TRACE FORMULAS

Below we summarize trace formulas for the various nonequilibrium quantities (17). The expressions are given both in the general operator notation, and in spherical wave representation in which the $\mathbb{T}$ operator and $\mathbb{G}_0$ become (infinitely dimensional) matrices $\mathcal{T}$ and $\mathcal{U}$.

Heat Radiation of One Object

The heat emitted by a body with T-matrix $\mathbb{T}$ at temperature T is given by (with $\mathcal{S} = \mathcal{I} + 2\mathcal{T}$)

$$H = \frac{2\hbar}{\pi}\int_0^\infty \mathrm{d}\omega \frac{\omega}{e^{\frac{\hbar\omega}{k_B T}}-1}\mathrm{Tr}\left[\mathrm{Im}(\mathbb{G}_0)\mathrm{Im}(\mathbb{T}) - \mathrm{Im}(\mathbb{G}_0)\mathbb{T}\,\mathrm{Im}(\mathbb{G}_0)\mathbb{T}^*\right] = \frac{\hbar}{2\pi}\int \mathrm{d}\omega \frac{\omega}{e^{\frac{\hbar\omega}{k_B T}}-1}\mathrm{Tr}\left(\mathcal{I} - \mathcal{S}\mathcal{S}^\dagger\right) \tag{38}$$

Heat Transfer Between Two Objects

The radiation emitted by body 1 at temperature T_1 and absorbed by body 2 is given by the transfer rate

$$H_1^{(2)} = \frac{2\hbar}{\pi}\int_0^\infty \mathrm{d}\omega \frac{\omega}{e^{\frac{\hbar\omega}{k_B T_1}}-1}\mathrm{Tr}\left\{\left[\mathrm{Im}(\mathbb{T}_2) - \mathbb{T}_2^*\,\mathrm{Im}(\mathbb{G}_0)\mathbb{T}_2\right]\frac{1}{1-\mathbb{G}_0\mathbb{T}_1\mathbb{G}_0\mathbb{T}_2}\mathbb{G}_0\left[\mathrm{Im}(\mathbb{T}_1) - \mathbb{T}_1\,\mathrm{Im}(\mathbb{G}_0)\mathbb{T}_1^*\right]\mathbb{G}_0^*\frac{1}{1-\mathbb{T}_2^*\mathbb{G}_0^*\mathbb{T}_1^*\mathbb{G}_0^*}\right\}$$

$$= \frac{2\hbar}{\pi}\int_0^\infty \mathrm{d}\omega \frac{\omega}{e^{\frac{\hbar\omega}{k_B T_1}}-1}\mathrm{Tr}\left[\left(\frac{\mathcal{T}_2^\dagger + \mathcal{T}_2}{2} + \mathcal{T}_2^\dagger\mathcal{T}_2\right)\frac{1}{\mathcal{I}-\mathcal{U}\mathcal{T}_1\mathcal{U}\mathcal{T}_2}\mathcal{U}\left(\frac{\mathcal{T}_1^\dagger + \mathcal{T}_1}{2} + \mathcal{T}_1\mathcal{T}_1^\dagger\right)\frac{1}{\mathcal{I}-\mathcal{U}^\dagger\mathcal{T}_2^\dagger\mathcal{U}^\dagger\mathcal{T}_1^\dagger}\mathcal{U}^\dagger\right]$$

Nonequilibrium Force Between Two Objects

The total force on body 2 is given by

$$\mathbf{F}^{(2)} = \mathbf{F}^{(2,\mathrm{eq})}(T_{\mathrm{env}}) + \sum_{\alpha=1,2}\left[\mathbf{F}_\alpha^{(2)}(T_\alpha) - \mathbf{F}_\alpha^{(2)}(T_{\mathrm{env}})\right]$$

where the first term is the usual equilibrium force (14–17) and

$$\mathbf{F}_1^{(2)}(T) = \frac{2\hbar}{\pi}\int_0^\infty \mathrm{d}\omega \frac{1}{e^{\frac{\hbar\omega}{k_B T}}-1}\mathrm{Re}\,\mathrm{Tr}\left\{\boldsymbol{\nabla}(1+\mathbb{G}_0\mathbb{T}_2)\frac{1}{1-\mathbb{G}_0\mathbb{T}_1\mathbb{G}_0\mathbb{T}_2}\mathbb{G}_0\left[\mathrm{Im}(\mathbb{T}_1) - \mathbb{T}_1\mathrm{Im}(\mathbb{G}_0)\mathbb{T}_1^*\right]\mathbb{G}_0^*\frac{1}{1-\mathbb{T}_2^*\mathbb{G}_0^*\mathbb{T}_1^*\mathbb{G}_0^*}\mathbb{T}_2^*\right\}$$

$$= \frac{2\hbar}{\pi}\int_0^\infty \mathrm{d}\omega \frac{1}{e^{\frac{\hbar\omega}{k_B T}}-1}\mathrm{Im}\,\mathrm{Tr}\left[\left(\mathcal{T}_2^\dagger\mathbf{p} + \mathcal{T}_2^\dagger\mathbf{p}\mathcal{T}_2\right)\frac{1}{\mathcal{I}-\mathcal{U}\mathcal{T}_1\mathcal{U}\mathcal{T}_2}\mathcal{U}\left(\frac{\mathcal{T}_1^\dagger + \mathcal{T}_1}{2} + \mathcal{T}_1\mathcal{T}_1^\dagger\right)\mathcal{U}^\dagger\frac{1}{\mathcal{I}-\mathcal{T}_2^\dagger\mathcal{U}^\dagger\mathcal{T}_1^\dagger\mathcal{U}^\dagger}\right]$$

$$\mathbf{F}_2^{(2)}(T) = \frac{2\hbar}{\pi}\int_0^\infty \mathrm{d}\omega \frac{1}{e^{\frac{\hbar\omega}{k_B T}}-1}\mathrm{Re}\,\mathrm{Tr}\left\{\boldsymbol{\nabla}(1+\mathbb{G}_0\mathbb{T}_1)\frac{1}{1-\mathbb{G}_0\mathbb{T}_2\mathbb{G}_0\mathbb{T}_1}\mathbb{G}_0\left[\mathrm{Im}(\mathbb{T}_2) - \mathbb{T}_2\mathrm{Im}(\mathbb{G}_0)\mathbb{T}_2^*\right]\frac{1}{1-\mathbb{G}_0^*\mathbb{T}_1^*\mathbb{G}_0^*\mathbb{T}_2^*}\right\}$$

$$= \frac{2\hbar}{\pi}\int_0^\infty \mathrm{d}\omega \frac{1}{e^{\frac{\hbar\omega}{k_B T}}-1}\mathrm{Im}\,\mathrm{Tr}\left[\left(\mathbf{p}\mathcal{U}\mathcal{T}_1\mathcal{U} + \mathbf{p}\right)\frac{1}{\mathcal{I}-\mathcal{T}_2\mathcal{U}\mathcal{T}_1\mathcal{U}}\left(\frac{\mathcal{T}_2^\dagger + \mathcal{T}_2}{2} + \mathcal{T}_2\mathcal{T}_2^\dagger\right)\frac{1}{\mathcal{I}-\mathcal{U}^\dagger\mathcal{T}_1^\dagger\mathcal{U}^\dagger\mathcal{T}_2^\dagger}\right],$$

where the translation operator $\mathbf{p}$ is defined by $-\boldsymbol{\nabla}_{\mathbf{d}}\mathcal{U}(\mathbf{d}) = \mathbf{p}\mathcal{U}$. The force on body 1 is obtained by exchanging the indices 1 and 2 in the equations above.

5. SIZE, SHAPE, AND GEOMETRY

5.1. Radiation

Thermal wavelength, λ_T: The dominant wavelength in the Planck radiation spectrum

According to classical theory of blackbody radiation, the thermal emission H of a macroscopic, isolated object at temperature T is proportional to its surface area A, as (2, 124)

$$\frac{H}{A} = \sigma T^4 \epsilon(T), \tag{39}$$

with $\sigma = \pi^2 k_B^4/(60\hbar^3 c^2)$ the Stefan–Boltzmann constant. The emissivity ϵ is in general a function of temperature. Equation 39 accurately describes the energy emitted if the object (and its radii of curvature) is large compared to the emitted wavelengths, centered around the thermal wavelength λ_T—in other words when, from the perspective of the wave, the surface is nearly flat. [Note that we neglect here the issue of view factors, which give a correction to Equation 39 due to shape, when part of the object's radiation is reabsorbed by itself (for a surface like in a ring).] Apart from concavity, Equation 39 turns inaccurate if the size of the object is comparable or small compared to λ_T. The radiation can then strongly depend on the materials in combination with shape, as we aim to demonstrate with two standard examples: a sphere and a cylinder (wire) of infinite length.

We start with a sphere made of glass (specifically, SiO_2), which is a good absorbing (and emitting) material, with otherwise mild optical properties. Its radiation, as a function of radius, is depicted in **Figure 3** (17, 24). For large R, the radiation indeed approaches the value given by Equation 39, where the emissivity of the glass chosen is $\epsilon = 0.735$. The important length scale is indeed λ_T, so that approach to Equation 39 is observed for $R \gg \lambda_T$. In the extreme of small R, the emitted energy is not proportional to surface area A but proportional to volume (note that the y-axis is normalized by A). This can be understood, as in this limit, the sphere is almost transparent, so that radiation emitted by any volume element contributes. This is in contrast to a large sphere, where only volume elements close to the surface contribute, as the emission from elements deeper inside is reabsorbed before reaching the surface.

Due to the plain optical properties of glass, its radiation in **Figure 3** is rather featureless, crossing over between the above two limits. More complex behavior is observed for good conductors such as gold (17). As seen in **Figure 3** the radiation of a gold sphere follows a similar trend for large R, approaching Equation 39 in the same manner as glass (only with the much smaller emissivity of $\epsilon = 0.0075$). For small R, the form is, however, very different compared to glass, and emission proportional to volume is not observed for any relevant values of R. Instead, for a pronounced range in R, the emission is proportional to R^5, i.e., volume to the power of 5/3. Although the origin of this dependence is nontrivial (related to the mathematical expansion of the Mie coefficients), the physical reason for absence of volume scaling is the short skin depth δ: Inside matter, the waves are damped as a function of position x with $\sim e^{-x/\delta}$, so that emission is dominated by regions within a width δ from the surface. For glass, typical values for δ (which depends on wavelength) are in the micron range: Scaling proportional to volume is observed if R is well below such scale. For gold, waves are damped much quicker, δ is on the order of a few nanometers, and the regime of volume-emission is shifted to much smaller R (not visible in the graph). Thus, thermal emission of micron- or nanoscale objects is largely controlled by the length scales λ_T and δ.

Turning to the cylinder of infinite length, **Figure 3** shows the emission of a glass cylinder as a function of its radius R (24, 125). The curve is very similar to that of a sphere, approaching the macroscopic law of Equation 39 for $R \gg \lambda_T$ while being proportional to volume for small R. Also the absolute values are very similar to the sphere, and the mildness of optical properties of glass is manifested once more by the weak sensitivity to shape. For gold (125), the situation is very different: While for $R \gg \lambda_T$ sphere and cylinder emit similarly, the curves are quite distinct for smaller radii. Here, the cylinder emission increases strongly and even exceeds the value of unity;

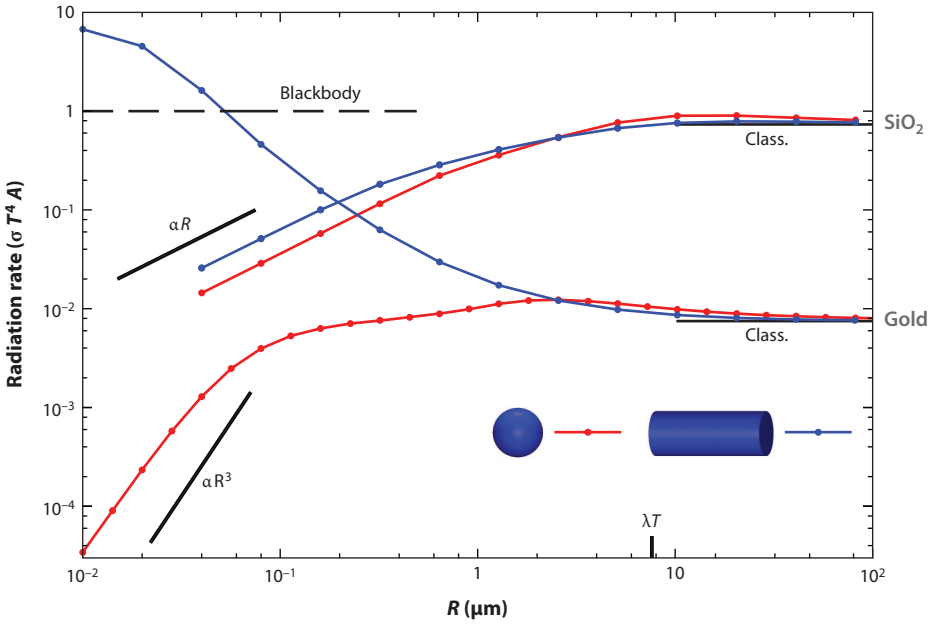

Figure 3

Thermal radiation of an isolated sphere (*red curves*) or cylinder of infinite length (*blue*), made of glass (SiO_2) or gold, at temperature $T = 300$ K, as a function of radius R. Horizontal lines on the right show results for $R \to \infty$, from Equation 39 with emissivities $\epsilon = 0.735$ for SiO_2 and $\epsilon = 0.0075$ for gold. Curves are normalized by the blackbody result, where A is the surface area. The experimental setup in the top row of **Figure 1** corresponds to $R = 0.5$ μm in the upper blue curve. The emitted radiation can be polarized, most notably for $R \ll \lambda_T$ (not shown) (24, 125). Data taken from References 17, 24, and 125. Bars denoted "Class." give the asymptotic value for large R.

i.e., it exceeds the emission of a blackbody. (Although the emissivity of any planar surface is bound from above by that of a blackbody, the curve in **Figure 3** does not violate any fundamental law, as it describes a body of finite size.) This strong emissivity is remarkable, as, e.g., for $R = 10$ nm, the gold cylinder exceeds the gold sphere by a factor $\sim 10^5$ in terms of emission, so that for gold, the emitted energy depends strongly on shape.

The experimental setup displayed in **Figure 1*a*** (18) consists of an SiO_2 nanofiber of radius 500 nm, as in **Figure 3**. The value of the experimental R is close to the regime where radiation is proportional to volume, thus distinctly different from the Stefan–Boltzmann law, as observed in Reference 18. The theoretical prediction in the graph in **Figure 1** was obtained with Equation 38.

Finally, we note that the radiation emitted by a cylinder is in general polarized. Regarding **Figure 3**, the polarization with electric fields parallel to the cylinder axis is dominant for small R [for gold the degree of polarization reaches nearly 1 (125)], whereas for $R \approx \lambda_T$, the perpendicular component can be stronger in intensity in some cases. This effect has been observed in several experiments including References 23, 126, and 127.

5.2. Radiative Energy Transfer

Given that radiation from an isolated object is very different from Equation 39, when the object is small or comparable with the thermal wavelength, it is expected that the radiative energy transfer between two objects should also be sensitive to their separation relative to λ_T. Indeed due to near-field effects heat transfer can be strongly enhanced (29). This is demonstrated in **Figure 4** for the

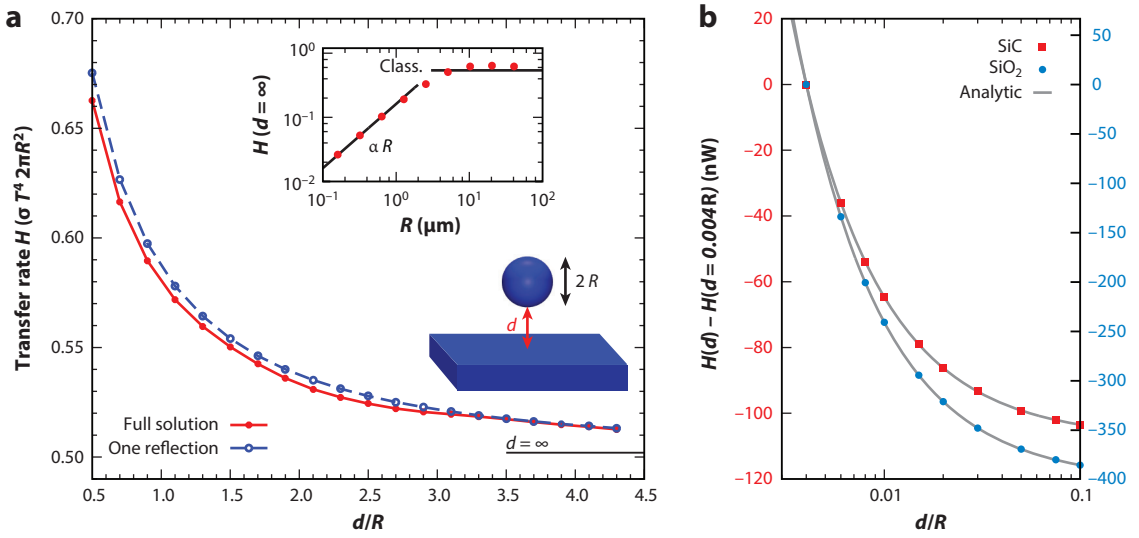

Figure 4

(*a*) Heat transfer rate (normalized to the Stefan–Boltzmann law) from a room temperature plate to a sphere at $T = 0$ of radius $R = 5$ μm (both SiO_2), as a function of separation; the horizontal bar shows the limit $d \to \infty$. The inset shows the result at large separation as a function of R. (*b*) Precision results for the same geometry, sphere, and plate either of SiO_2 (*right abscissa*) or SiC (*left abscissa*), as a function of d. R is chosen very small (in the range of nanometers), so that the curve is only a function of d/R. Data points show numerical results from partial waves expansion, and solid lines give the analytical result from Equation 40. The relative deviation of numerical data to analytic curve is around 10^{-4}. Data taken from References 24 and 128.

case of a sphere opposite a planar surface, with both made of glass (SiO_2) (24). The radius of the sphere is $R = 5$ μm, and we measure distance d between the closest points on the surfaces. Indeed, for $d \gg \lambda_T$, the transferred energy approaches a distance-independent value. This value, although obtained for large separations, is still a nontrivial function of radius R and is strongly reminiscent of **Figure 3**: We see a regime where the transfer is proportional to the sphere's volume, and for $R \gg \lambda_T$, H is proportional to the sphere's surface area, as expected. The value of $H = \sigma T^4 \epsilon^2(T)$ (compare with Equation 39) is, however, not approached exactly.

In the continuum formulation, the heat transfer diverges with decreasing separation as $1/d$. From the experimental and technical perspective, it is important to understand the physical limitations of this unbounded growth. Experimental deviations from the form of this divergence, as predicted by FE, can provide valuable clues in this regard. The short distance divergence suggests a proximity approximation (PA) dominated by contributions at closest separation. Indeed, despite the fact that H is a complicated function of the parameters involved, the following analytical expansion is valid if the sphere is small compared to the skin depth δ (128),

$$H(d) = \frac{2\pi R\lambda}{d}\left[1 - (2\beta - 1)\frac{d}{R}\log\frac{d}{d_0}\right] + \mathcal{O}(d^0). \quad (40)$$

Proximity approximation (PA): expressing the result for curved surfaces in terms of the simpler result for parallel plates; exact in certain limits

This curve is shown in **Figure 4*b*** with exact numerical data, which was obtained by expansion in spherical waves and truncation at a multipole number of 2,500. The parameters α and β depend on materials and temperature and were computed independently (not fitted) (128). The scheme of PA (see also References 41, 43, and 129), which leads in general to results similar to Equation 40 (for cases where $R \ll \delta$ does not hold), has also proven useful in analysis of experimental data as, for example, given in **Figure 1*b***.

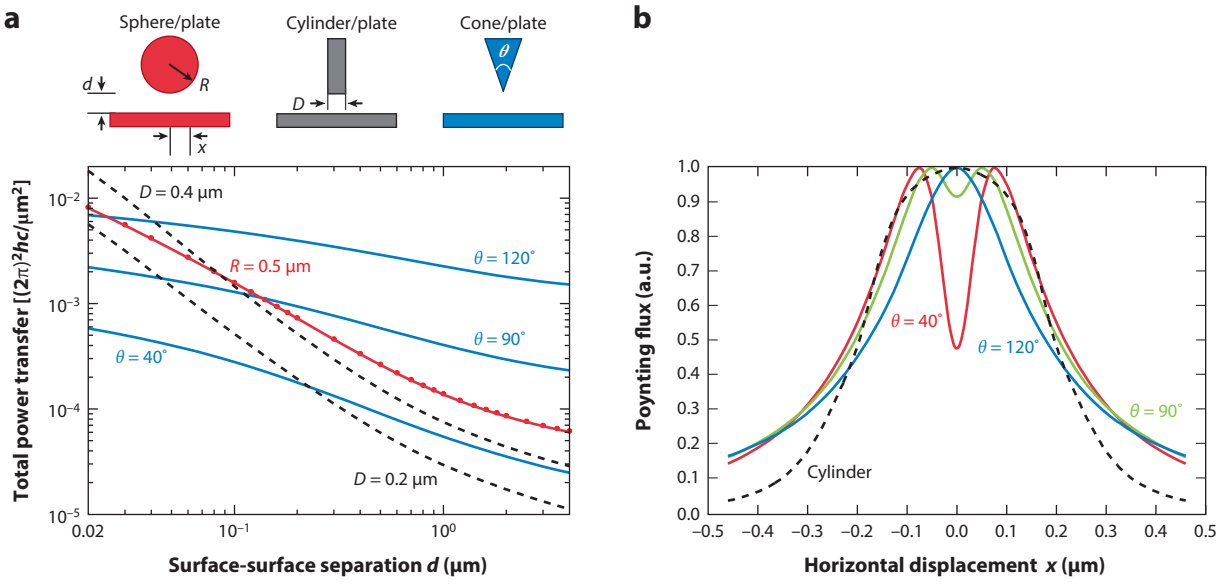

Figure 5

(*a*) Numerical results for radiative energy transfer for three setups (see sketch, colors of curves corresponding to colors of the sketch). Materials chosen are (marginally) different types of glass, and objects are at a temperature of 600 K, whereas the planar surface is kept at 300 K. (*b*) Spatially resolved heat transfer flux as a function of lateral position x on the planar surface. The dashed curve is for the cylinder, whereas the colored solid curves depict the cone at different opening angles. Surface-surface separation is 70 nm in all cases, and curves are normalized to a maximum of unity. Adapted from Reference 44 with permission.

Figure 5 shows radiative heat transfer between a planar surface and three different generic compact objects, a sphere, a cylinder, and a cone (44). These results were obtained from a numerical scattering scheme, where the surfaces are discretized and meshed. The value for the sphere approaches a $1/d$ law, in agreement with Equation 40, whereas the result for the cylinder asymptotically diverges with $1/d^2$, which is also in agreement with the PA. By contrast, the transfer between the plate and the sharp cone has a much less pronounced divergence; the numerics are consistent with a logarithmic dependence on d for small d. This is also in qualitative agreement with the PA. In panel *b*, the energy flux (Poynting flux) is shown in a spatially resolved manner, as a function of lateral position on the surface. This quantity gives the relative local heating strength of the surface, which may be important for thermal writing applications. The cylinder shows the expected result that the local heating is almost a step function with width corresponding to the diameter of the cylinder. An unexpected observation is made for the cone (which is the more dominant, the sharper the cone): The region right below the tip is actually a local minimum, whereas the maximal heat is absorbed a distance away from the center. This means that the hot cone, when brought close to the surface, does not heat the surface on a localized spot but rather on a ring around its tip: Although the tip is the point closest to the surface, the cone seems to emit energy predominantly on its side, so that the competition of these effects leads to the displaced maximum. Heat transfer in the cone plate geometry was measured in a recent experiment (37).

5.3. Casimir Force

For systems out of equilibrium, forces acting on the objects are also quite distinct from their equilibrium counterparts. The general features are demonstrated in **Figure 6**, where we show the forces

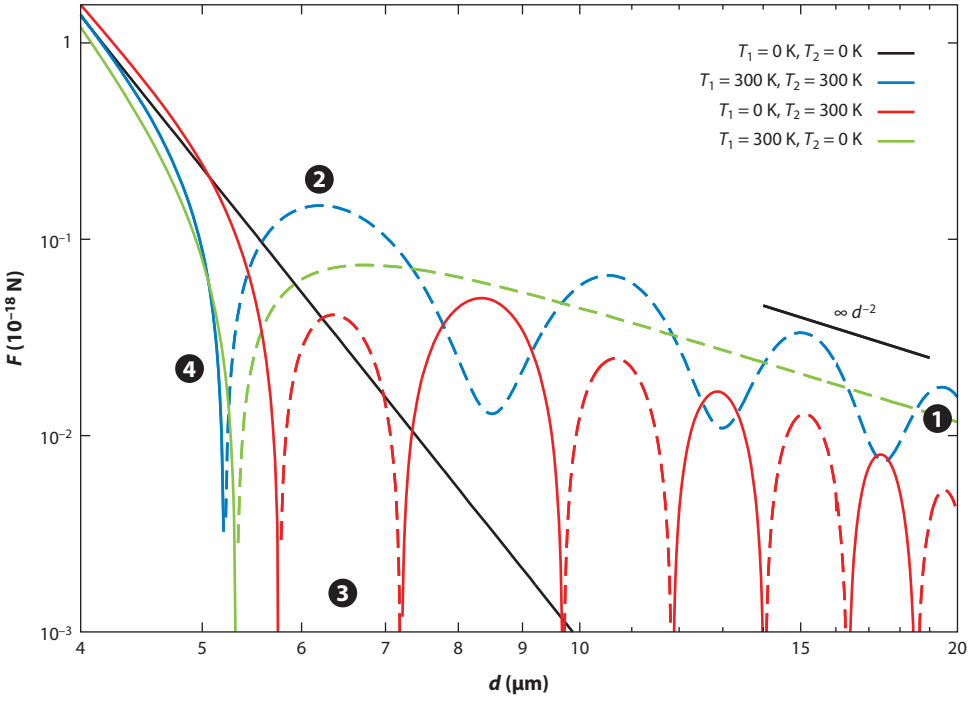

Figure 6

Nonequilibrium forces between two spheres (radii $R = 1$ μm, made of SiO_2) at center-to-center distance d, at temperatures as given. The environment is at 0 K, and only the black curve describes a global equilibrium state. Curves show the force acting on sphere 2, which is not equal and opposite to the force acting on the first sphere. Solid lines show attraction; dashed lines show repulsion. Four noticeable characteristics are marked with numbers. Adapted from Reference 6 with permission.

on two spheres at large separation. In equilibrium, this limit is referred to as the Casimir Polder regime (130). We note the following four remarkable differences to the case of equilibrium (6):

1. In equilibrium, the Casimir force between the spheres falls off with inverse distance to the 8th power (at zero temperature) or the 7th power (at finite temperature). If out of equilibrium, i.e., if the temperatures of the two spheres and the environment are not all equal, the behavior is drastically altered, and the force decays much slower, with the inverse distance to the second power (see **Figure 6**, ❶). This may be understood by contemplating the radiation pressure from photons.
2. The sign of the force, always attractive in equilibrium, can take either sign out of equilibrium. In the graph, we indicate repulsive forces by dashed lines, and attractive ones with solid lines. The ❷ denotes a regime where the force is repulsive.
3. In equilibrium, the Casimir force does not allow stable points; it is forbidden by a strict theorem (131). Also in this respect nonequilibrium is less restrictive: For a certain temperature combination, the force changes its sign several times, indicating that positions of zero force exist. Naturally, in every second zero, the force changes from repulsive to attractive; such points thus exhibit stability with a minimum at the corresponding potential. (See **Figure 6**, ❸.)
4. The graph shows the force acting on sphere 2 (**Figure 6**, ❷) for different combinations of temperatures. We first note that the forces on the spheres are generally not equal and

Force in equilibrium:

$$F^{\mathrm{eq}} = \frac{161}{4\pi}\frac{\hbar c}{d^8}\alpha_1\alpha_2$$

Force in equilibrium, finite temperature:

$$F^{\mathrm{eq}} = \frac{18\hbar c}{d^7\lambda_T}\alpha_1\alpha_2$$

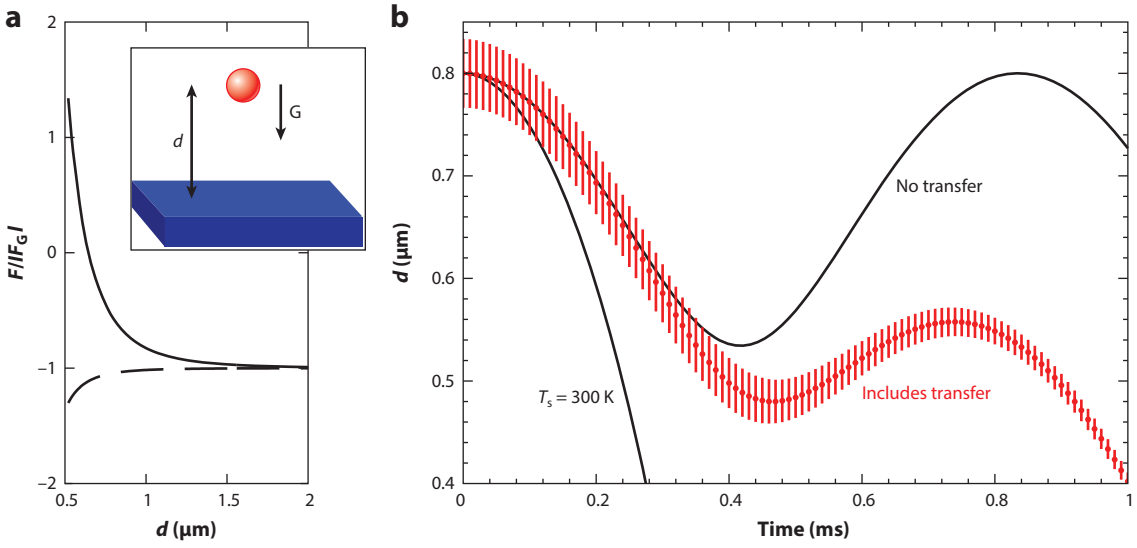

Figure 7

Casimir levitation. (*a*) A hot sphere ($T_s = 900$ K) is placed above a surface at room temperature. The panel shows the total force, including gravity, which, at a certain range of distances d, is repulsive. (*b*) The panel gives the trajectory of the sphere if dropped from a height of $d = 800$ nm: The sphere bounces on the surface, a motion eventually cut off by the cooling of the sphere. The red curve includes this effect, and the red envelope around the curve gives the temperature difference between the sphere and the surface in arbitrary units. Because the trajectory is distinctly different in equilibrium (the curve labeled $T_s = 300$ K), such a setup may provide an interesting manifestation of levitation due to out-of-equilibrium Casimir forces. Data taken from Reference 17.

opposite (as they are in equilibrium). This is possible, as photons that travel to, or come from, the surrounding environment carry momentum so that the forces on all objects in the system (including emitted and absorbed photons) still add up to zero. But staying with the example of a cold sphere (0 K) and a warm sphere (300 K) is illustrative, as then, the force acting on the cold one and the force acting on the warm one cross at $d \approx 6$ μm (**Figure 6**, ❹), where the forces acting on the two are equal in magnitude. The directions of forces are also equal, so that the cold sphere is repelled while the warm sphere is attracted. In this configuration, the spheres will thus start traveling in the same direction, keeping their distance constant, representing a self-propelled pair. Self propulsion through Casimir forces has been investigated in more detail in Reference 132.

Figure 6 demonstrates the general features of nonequilibrium Casimir forces and differences compared to equilibrium counterparts. However, the experimental measurement of the forces remains challenging, as they mostly dominate the total force at somewhat larger distances, $d \approx \lambda_T$, and are hence often overshadowed by the equilibrium forces. In **Figure 7**, we analyze a setup with potential experimental measurability (17): Here, a sphere (temperature 900 K) above a surface (temperature 300 K) is considered; both are made of a dielectric material and described by a typical Lorentz form (see Reference 17, p. 24 for details). Here, another pronounced difference of nonequilibrium phenomena compared to equilibrium ones comes into play: In equilibrium (mathematically apparent through the evaluation on the imaginary axis), the frequency dependence of the dielectric functions enters in a broadband manner, whereas out of equilibrium, resonances are important. As such, it is for example possible to tune the nonequilibrium force from attractive

to repulsive, by just tuning such resonances, especially, their relative positions (17, 87, 133, 134). This has been done (again, see Reference 17, p. 24, for details) so that the sphere feels the total force depicted in the left-hand side of the graph. The total force includes the gravitational force and the Casimir force which are opposite in direction. For decreasing d, the Casimir force, due to nonequilibrium, is repulsive, acting against gravity, and, around $\approx$0.7 μm, balances it. For smaller d, the total force is repulsive. For even smaller d, the equilibrium part of the force will eventually take over and render the total force attractive again. Nevertheless, at the zero force point around $d \approx 0.7$ μm, the sphere is in a local potential minimum. To make this statement even more obvious, we have in the right-hand graph shown various trajectories of the sphere, if initially at $d = 800$ nm (with zero velocity): The sphere will perform an oscillatory motion around the potential minimum, as illustrated. However, this curve gives an over-idealized situation, as in reality, the sphere will cool down, due to radiative heat transfer to the surface and the environment (predominantly to the surface). This effect is included in the red curve, showing that with decreasing temperature, the repulsive force weakens, and the sphere eventually drops on the surface. Here, width of the red envelope around the curve gives the temperature difference between the sphere and the surface in arbitrary units. Interestingly, the relaxation time of temperature, around 1 ms, is on the same order of magnitude as the period of positional oscillations of the sphere. Thus, the trajectory appears experimentally measurable, and most importantly, is distinctly different from the trajectory at equilibrium (as shown). Here, the Casimir force is attractive throughout, and, boosted by gravity, the sphere rapidly drops to the surface.

6. PERSPECTIVE

In this review we employed scattering theory along with Rytov's FE to describe and gain insights into several aspects of near-field heat radiation, heat transfer, and Casimir forces. There are certainly myriad applications of these results in submicron-scale devices, and precise experimental verification of nonequilibrium Casimir forces is lacking. There are, however, several avenues for future theoretical investigation:

- As noted in Section 2, a central assumption of Rytov's FE is that of local thermal equilibrium for each object. However, in real systems where temperatures of objects and environment differ substantially (e.g., hot objects in cold environment), the assumption of temperature homogeneity within each object is questionable. Hence, it would be of both theoretical and practical importance to extend the results to nonhomogeneous temperatures, taking into account material heat conductivities.
- Section 5 employed bulk dielectric functions to compute heat radiation and nonequilibrium Casimir forces at scales of tens of nanometres relevant to nanofibers. To justify the approach, it is necessary to find out how accurately bulk dielectric properties apply at small scales. At scales of a few angstroms, atomistic (band structure) calculations are likely needed, whereas at intermediate scales a wave number–dependent dielectric response may be sufficient.
- The problem of determining the correct magnitude of the thermal contribution to the Casimir force between two metallic plates is still waiting for a definitive resolution after twenty years of efforts. Although a theoretical resolution of the conundrum might require a fully microscopic quantum mechanical theory of fluctuation forces for conduction electrons, perhaps along the lines of Reference 76, it is hoped that an experimental clarification may be within reach based on a recently proposed differential measurement scheme (62–67).
- The computations described here rely heavily on the linear response of the bodies. It is interesting to generalize the result to the case of nonlinear EM response. Perturbative computations along this line are currently underway.

DISCLOSURE STATEMENT

The authors are not aware of any affiliations, memberships, funding, or financial holdings that might be perceived as affecting the objectivity of this review.

ACKNOWLEDGMENTS

M.K. was supported by the NSF through grant No. DMR-1206323. Ma.K. was supported by Deutsche Forschungsgemeinschaft (DFG) grant No. KR 3844/2-1 and MIT-Germany Seed Fund grant No. 2746830.

LITERATURE CITED

1. Planck M. 1901. *Ann. Phys. (NY)* 4:553
2. Boltzmann L. 1884. *Ann. Phys. (NY)* 22:291
3. Parsegian VA. 2006. *Van der Waals forces: A Handbook for Biologists, Chemists, Engineers, and Physicists*. Cambridge, UK: Cambridge Univ. Press
4. Casimir HBG. 1948. *Proc. K. Ned. Akad. Wet.* 51:793
5. Lifshitz EM. 1956. *Sov. Phys. J. Exp. Theoret. Phys.* 2:73
6. Krüger M, Emig T, Bimonte G, Kardar M. 2011. *Europhys. Lett.* 95:21002
7. Milonni W. 1994. *The Quantum Vacuum*. San Diego: Academic
8. Golyk VA. 2014. *Non-equilibrium fluctuation-induced phenomena in quantum electrodynamics*. PhD Thesis, Mass. Inst. Technol., Cambridge, MA
9. Pendry JB. 1999. *J. Phys.: Condens. Matter* 11:6621
10. Majumdar A. 1999. *Annu. Rev. Mater. Sci.* 29:505
11. Rytov SM, Kravtsov YA, Tatarskii VI. 1978. *Principles of Statistical Radiophysics 3*. Berlin: Springer
12. Bordag M, Klimchitskaya GK, Mohideen U, Mostepanenko VM. 2009. *Advances in the Casimir Effect*. Oxford, UK: Oxford Univ. Press
13. Antezza M, Pitaevskii LP, Stringari S, Svetovoy VB. 2008. *Phys. Rev. A* 77:022901
14. Emig T, Graham N, Jaffe RL, Kardar M. 2007a. *Phys. Rev. Lett.* 99:170403
15. Maia Neto PA, Lambrecht A, Reynaud S. 2008. *Phys. Rev. A* 78:012115
16. Rahi SJ, Emig T, Graham N, Jaffe RL, Kardar M. 2009. *Phys. Rev. D* 80:085021
17. Krüger M, Bimonte G, Emig T, Kardar M. 2012. *Phys. Rev. B* 86:115423
18. Wuttke C, Rauschenbeutel A. 2013. *Phys. Rev. Lett.* 111:024301
19. Shen S, Narayanaswamy A, Chen G. 2009. *Nano Lett.* 9:2909
20. Banishev AA, Wagner J, Emig T, Zandi R, Mohideen U. 2013a. *Phys. Rev. Lett.* 110:250403
21. Rytov SM. 1959. *Theory of Electric Fluctuations and Thermal Radiation*. Bedford, MA: Air Force Cambridge Res. Cent.
22. Singer SB, Mecklenburg M, White ER, Regan BC. 2011. *Phys. Rev. B* 83:233404
23. Bimonte G, Cappellin L, Carugno G, Ruoso G, Saadeh D. 2009. *New J. Phys.* 11:033014
24. Krüger M, Emig T, Kardar M. 2011. *Phys. Rev. Lett.* 106:210404
25. Kattawar GW, Eisner M. 1970. *Appl. Opt.* 9:2685
26. Bohren CF, Huffmann DR. 2004. *Absorption and Scattering of Light by Small Particles*. Weinheim, Ger.: Wiley
27. Hansen K, Campbell EEB. 1998. *Phys. Rev. E* 58:5477
28. Ruan Z, Fan S. 2010. *Phys. Rev. Lett.* 105:013901
29. Polder D, Van Hove M. 1971. *Phys. Rev. B* 4:3303
30. Hargreaves CM. 1969. *Phys. Lett. A* 30:491
31. Domoto GA, Boehm RF, Tien CL. 1970. *J. Heat Transf.* 92:412
32. Narayanaswamy A, Chen G. 2008a. *Phys. Rev. B* 78:115303
33. Kittel A, Müller-Hirsch W, Parisi J, Biehs S-A. 2005. *Phys. Rev. Lett.* 95:224301
34. de Wilde Y, Formanek F, Carminati R, Gralak B, Lemoine PA, et al. 2006. *Nature* 444:740

35. Rousseau E, Siria A, Jourdan G, Volz S, Comin F, et al. 2009. *Nat. Photonics* 3:514
36. Ottens RS, Quetschke V, Wise S, Alemi AA, Lundock R, et al. 2011. *Phys. Rev. Lett.* 107:014301
37. Kim K, Song B, Fernandez-Hurtado V, Lee W, Jeong W, et al. 2015. *Nature* 528:387
38. Loomis JJ, Maris HJ. 1994. *Phys. Rev. B* 50:18517
39. Biehs SA, Greffet JJ. 2010. *Phys. Rev. B* 82:245410
40. Volokitin AI, Persson BNJ. 2001. *Phys. Rev. B* 63:205404
41. Otey C, Fan S. 2011. *Phys. Rev. B* 84:245431
42. Domingues G, Volz S, Joulain K, Greffet JJ. 2005. *Phys. Rev. Lett.* 94:085901
43. Narayanaswamy A, Chen G. 2008b. *Phys. Rev. B* 77:075125
44. McCauley AP, Reid MTH, Krüger M, Johnson SG. 2012. *Phys. Rev. B* 85:165104
45. Bimonte G. 2009a. *Phys. Rev. A* 80:042102
46. Messina R, Antezza M. 2011a. *Europhys. Lett.* 95:61002
47. Messina R, Antezza M. 2011b. *Phys. Rev. A* 84:042102
48. Rodriguez AW, Reid MTH, Johnson SG. 2012. *Phys. Rev. B* 86:220302
49. Polimeridis AG, Reid MTH, Jin W, Johnson SG, White JK, Rodriguez AW. 2015. *Phys. Rev. B* 92:134202
50. Huth O, Rüting F, Biehs S, Holthaus M. 2010. *Eur. Phys. J. Appl. Phys.* 50
51. Incardone R, Emig T, Krüger M. 2014. *Europhys. Lett.* 106:41001
52. Lamoreaux SK. 1997. *Phys. Rev. Lett.* 78:5
53. Mohideen U, Roy A. 1998. *Phys. Rev. Lett.* 81:4549
54. Bressi G, Carugno G, Onofrio R, Ruoso G. 2002. *Phys. Rev. Lett.* 88:041804
55. Milton KA. 2001. *The Casimir Effect: Physical Manifestations of Zero-Point Energy*. Singapore: World Sci.
56. Mostepanenko VM, Trunov NN. 1997. *The Casimir Effect and Its Applications*. Oxford, UK: Clarendon
57. Dalvit D, Milonni P, Roberts D, da Rosa F, eds. 2011. *Casimir Physics*. Berlin/Heidelberg, Ger.: Springer-Verlag
58. Rodriguez AW, Capasso F, Johnson SJ. 2011. *Nat. Photonics* 5:211
59. Antezza M, Pitaevskii LP, Stringari S. 2005. *Phys. Rev. Lett.* 95:113202
60. Obrecht JM, Wild RJ, Antezza M, Pitaevskii LP, Stringari S, Cornell EA. 2007. *Phys. Rev. Lett.* 98:063201
61. Antezza M, Pitaevskii LP, Stringari S, Svetovoy VB. 2006. *Phys. Rev. Lett.* 97:223203
62. Bimonte G. 2014a. *Phys. Rev. Lett.* 112:240401
63. Bimonte G. 2014b. *Phys. Rev. Lett.* 113:240405
64. Bimonte G. 2015a. *Phys. Rev. B* 91:205443
65. Bimonte G. 2015b. *Phys. Rev. A* 92:025028
66. Decca RS. 2016. *Int. J. Mod. Phys. A* 31:1641024
67. Bimonte G, Lopez D, Decca RS. 2016. *Phys. Rev. B* 93:184434
68. Rytov S. 1958. *Sov. Phys. J. Exp. Theoret. Phys.* 6:130
69. Callen HB, Welton TA. 1951. *Phys. Rev.* 83:34
70. Agarwal G. 1975. *Phys. Rev. A* 11:230
71. Bimonte G, Santamato E. 2007. *Phys. Rev. A* 76:013810
72. Landau L, Lifshitz E. 1963. *Electrodynamics of Continuous Media*. Oxford, UK: Pergamon
73. Kats EI. 1977. *Sov. Phys. J. Exp. Theoret. Phys.* 46:109
74. Milton KA, Brevik I, Ellingsen SA. 2012. *Phys. Scr. T* 151:014070
75. Bezerra VB, Klimchitskaya GL, Mostepanenko VM. 2002. *Phys. Rev. A* 66:052113
76. Buenzli PR, Martin PA. 2008. *Phys. Rev. E* 77:011114
77. Bimonte G. 2009b. *Phys. Rev. A* 79:042107
78. Intravaia F, Henkel C. 2009. *Phys. Rev. Lett.* 103:130405
79. Banishev AA, Klimchitskaya GL, Mostepanenko VM, Mohideen U. 2013b. *Phys. Rev. Lett.* 110:137401
80. Decca RS, López D, Fischbach E, Klimchitskaya GL, Krause DE, Mostepanenko VM. 2005. *Ann. Phys. (NY)* 318:37
81. Decca RS, López D, Fischbach E, Klimchitskaya GL, Krause DE, Mostepanenko VM. 2007. *Eur. Phys. J. C* 51:963
82. Sushkov AO, Kim WJ, Dalvit DAR, Lamoreaux SK. 2011. *Nat. Phys.* 7:230
83. Joulain K, Mulet J-P, Marquier F, Carminati R, Greffet J-J. 2005. *Surf. Sci. Rep.* 57:59–112
84. Volokitin AI, Persson BNJ. 2007. *Rev. Mod. Phys.* 79:1291

85. Challener WA, Peng C, Itagi AV, Karns D, Peng W, et al. 2009. *Nat. Photonics* 3:220
86. Basu S, Zhang ZM, Fu CJ. 2009. *Int. J. Energy Res.* 33:1203
87. Bimonte G, Emig T, Krüger M, Kardar M. 2011. *Phys. Rev. A* 84:042503
88. Waterman PC. 1971. *Phys. Rev. D* 3:825
89. Langbein D. 1974. *Theory of van der Waals Attraction*. Heidelberg, Ger.: Springer
90. Jaekel MT, Reynaud S. 1991. *J. Phys. I* 1:1395
91. Genet C, Lambrecht A, Reynaud S. 2003. *Phys. Rev. A* 67:043811
92. Lambrecht A, Maia Neto PA, Reynaud S. 2006. *New J. Phys.* 8:243
93. Balian R, Duplantier B. 1977. *Ann. Phys (NY)* 104:300
94. Balian R, Duplantier B. 1978. *Ann. Phys. (NY)* 112:165
95. Krein MG. 1953. *Mat. Sborn. (NS)* 33:597
96. Krein MG. 1962. *Sov. Math. Dokl.* 3:707
97. Birman MS, Krein MG. 1962. *Sov. Math. Dokl.* 3:740
98. Henseler M, Wirzba A, Guhr T. 1997. *Ann. Phys. (NY)* 258:286
99. Wirzba A. 1999. *Phys. Rep.* 309:1
100. Bulgac A, Wirzba A. 2001. *Phys. Rev. Lett.* 87:120404
101. Bulgac A, Magierski P, Wirzba A. 2006. *Phys. Rev. D* 73:025007
102. Wirzba A. 2008. *J. Phys. A: Math. Theor.* 41:164003
103. Bordag M, Robaschik D, Wieczorek E. 1985. *Ann. Phys. (NY)* 165:192–213
104. Robaschik D, Scharnhorst K, Wieczorek E. 1987. *Ann. Phys. (NY)* 174:401–29
105. Li H, Kardar M. 1991. *Phys. Rev. Lett.* 67:3275–78
106. Li H, Kardar M. 1992. *Phys. Rev. A* 46:6490–500
107. Emig T, Hanke A, Golestanian R, Kardar M. 2001. *Phys. Rev. Lett.* 87:260402
108. Emig T, Hanke A, Golestanian R, Kardar M. 2003. *Phys. Rev. A* 67:022114
109. Büscher R, Emig T. 2005. *Phys. Rev. Lett.* 94:133901
110. Kenneth O, Klich I. 2006. *Phys. Rev. Lett.* 97:160401
111. Emig T, Graham N, Jaffe RL, Kardar M. 2007b. *Phys. Rev. Lett.* 99:170403
112. Emig T, Graham N, Jaffe RL, Kardar M. 2008. *Phys. Rev. D* 77:025005
113. Schwinger J. 1975. *Lett. Math. Phys.* 1:43
114. Kenneth O, Klich I. 2008. *Phys. Rev. B* 78:014103
115. Milton KA, Parashar P, Wagner J. 2008a. *Phys. Rev. Lett.* 101:160402
116. Reid MTH, Rodriguez AW, White J, Johnson SG. 2009. *Phys. Rev. Lett.* 103:040401
117. Golestanian R. 2009. *Phys. Rev. A* 80:012519
118. Ttira CC, Fosco CD, Losada EL. 2010. *J. Phys. A* 43:235402
119. Teo L. 2013. *Phys. Rev. D* 88:045019
120. Fosco CD, Lombardo FC, Mazzitelli FD. 2011. *Phys. Rev. D* 84:105031
121. Bimonte G, Emig T, Jaffe RL, Kardar M. 2012. *Europhys. Lett.* 97:50001
122. Bimonte G, Emig T, Kardar M. 2012. *Appl. Phys. Lett.* 100:074110
123. Derjaguin BV, Abrikosova II. 1957. *Sov. Phys. J. Exp. Theoret. Phys.* 3:819
124. Stefan J. 1879. *Sitz. Math.-Naturwiss. Cl. Kais. Akad. Wiss.* 79:391–428
125. Golyk VA, Krüger M, Kardar M. 2012. *Phys. Rev. E* 85:046603
126. Öhman Y. 1961. *Nature* 192:254
127. Borghesani A, Carugno G. 2016. *Int. J. Therm. Sci.* 104:101
128. Golyk VA, Krüger M, McCauley AP, Kardar M. 2013. *Europhys. Lett.* 101:34002
129. Sasihithlu K, Narayanaswamy A. 2011. *Phys. Rev. B.* 83:161406
130. Boyer TH. 1975. *Phys. Rev. A* 11:1650
131. Rahi S, Kardar M, Emig T. 2010. *Phys. Rev. Lett.* 105:070404
132. Müller B, Krüger M. 2016. *Phys. Rev. A* 93:032505
133. Henkel C, Joulain K, Mulet JP, Greffet JJ. 2002. *J. Opt. A: Pure Appl. Opt.* 4:S109
134. Cohen AE, Mukamel S. 2003. *Phys. Rev. Lett.* 91:233202

Annual Review
of Condensed
Matter Physics

Volume 8, 2017

Contents

Errata

An online log of corrections to *Annual Review of Condensed Matter Physics* articles may be found at http://www.annualreviews.org/errata/conmatphys